

## Structure–Property Correlations in Model Compounds of Oligomer Liquid Crystals

Yuji Sasanuma,<sup>\*,†</sup> Tetsushi Ono,<sup>†</sup> Yoshihiko Kuroda,<sup>†</sup> Emi Miyazaki,<sup>†</sup> Ken Hikino,<sup>†</sup> Jun Arou,<sup>†</sup> Kohji Nakata,<sup>†</sup> Hideaki Inaba,<sup>‡</sup> Ken-ichi Tozaki,<sup>‡</sup> Hideko Hayashi,<sup>‡</sup> and Kentaro Yamaguchi<sup>§</sup>

Department of Materials Technology, Faculty of Engineering, Faculty of Education, and The Chemical Analysis Center, Chiba University, 1-33 Yayoi-cho, Inage-ku, Chiba 263-8522, Japan

Received: February 16, 2004; In Final Form: May 25, 2004

Structure–property correlations of the following model compounds for oligomer liquid crystals (LCs) have been investigated: monomers,  $C_6H_5O(CH_2)_xCH_3$  ( $x = 4$  and  $5$ ); dimers,  $C_6H_5O(CH_2)_xOC_6H_5$  ( $x = 3, 4, 5,$  and  $6$ ); and tetramers,  $C_6H_5O(CH_2)_xOC_6H_4O(CH_2)_xOC_6H_4O(CH_2)_xOC_6H_5$  ( $x = 5$  and  $6$ ). Deuterium NMR quadrupolar splittings observed from the deuterated model compounds dissolved in a nematic solvent, 4'-methoxybenzylidene-4-*n*-butylaniline (MBBA) or *p*-azoxyanisole (PAA), were analyzed by the rotational isomeric state scheme with the maximum entropy method to yield the orientational order parameters, bond conformations, and molecular dimensions. For the dimers in particular, the solute shapes were estimated from phase diagrams of the dimer/MBBA systems, the crystal structures were determined by X-ray diffraction, and the melting points and enthalpies of fusion were evaluated from DSC measurements. From the dimers, the so-called odd–even effect was clearly observed in not only the orientational order and molecular shape in the nematic solution but also the crystal structure and thermal properties; that is, the dimers of  $x = 4$  and  $6$  have larger order parameters, more anisotropic shapes, better-arranged crystal structures, higher melting points, and larger enthalpies of fusion than those of  $x = 3$  and  $5$ . In the nematic solution, the model compounds preserve the inherent conformational preferences of the ether chain and enhance the shape anisotropy by increasing the trans fractions. As the orientational correlation is expected to persist only within a short range, conformations of the tetramers may represent those of polymer LCs with the same ethereal spacers. The chainlike molecules adjust their spatial configuration to the LC environment, and consequently, physical properties of the LC system are affected.

## 1. Introduction

If the concept of liquid crystallinity is defined as a capability of compounds to form liquid crystalline phases by themselves (liquid crystallinity in a narrow sense), such properties are often found for compounds with a rigid (mesogen) component or an alternation of rigid and flexible (tail or spacer) components:<sup>1,2</sup> for example, 4'-methoxybenzylidene-4-*n*-butylaniline (MBBA, Figure 1a), *p*-azoxyanisole (PAA, Figure 1b), 4'-*n*-alkoxy-4-cyanobiphenyl,  $\alpha,\omega$ -bis[(4,4'-cyanobiphenyl)oxy]alkanes (CBA- $x$ ,  $x$  is the number of spacer carbons). These compounds have been referred to as liquid crystals (LCs).

If a nematic LC is mixed with a nonrigid solute, the nematic-to-isotropic (NI) transitional temperature ( $T_{NI}$ ) of the pure LC is lowered, and a two-phase region is formed between  $T_N$  and  $T_I$ : On heating, the isotropic phase appears at  $T_N$ , and the nematic phase completely disappears at  $T_I$ . The ability of the solute to destabilize the nematic phase is represented by the slopes ( $\beta_N$  and  $\beta_I$ ) of the ( $T_N^*$ ,  $x_2$ ) and ( $T_I^*$ ,  $x_2$ ) boundaries in the  $T^*$  ( $=T/T_{NI}$ ) versus  $x_2$  (molar fraction of solute) plot.<sup>3–7</sup> In Figure 2, the  $\beta_N^\infty$  values of various compounds dissolved in a nematic solvent, MBBA, obtained by extrapolation of the  $\beta_N$ 's to the infinity dilution, are plotted against core volumes ( $V_2^*$ )s

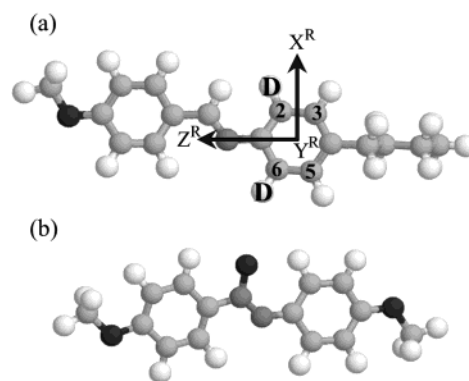


**Figure 1.** Nematic solvents used in this study: (a) 4'-methoxybenzylidene-4-*n*-butylaniline (MBBA) and (b) *p*-azoxyanisole (PAA). For MBBA, the  $X^R$ ,  $Y^R$ , and  $Z^R$  axes are defined as shown.

of the solutes. The  $\beta_N^\infty$  values of the branched molecules increase with  $V_2^*$ , whereas those of the *n*-alkanes appear to be invariant. The globular solutes are shown to disturb the nematic order more effectively than the *n*-alkanes; therefore, chain molecules are suggested to be closer to LCs than spherical ones. If we extend the concept of liquid crystallinity to a capability of molecules to adapt themselves to liquid crystalline phases (liquid crystallinity in a broad sense), we can consider that all compounds possess this property to a greater or lesser extent. Figure 2 shows that the *n*-alkanes are superior in liquid crystallinity to the branched molecules.

\* To whom correspondence should be addressed. E-mail: sasanuma@faculty.chiba-u.jp. Fax: +81 43 290 3394.

<sup>†</sup> Department of Materials Technology, Faculty of Engineering.

<sup>‡</sup> Faculty of Education.

<sup>§</sup> The Chemical Analysis Center.

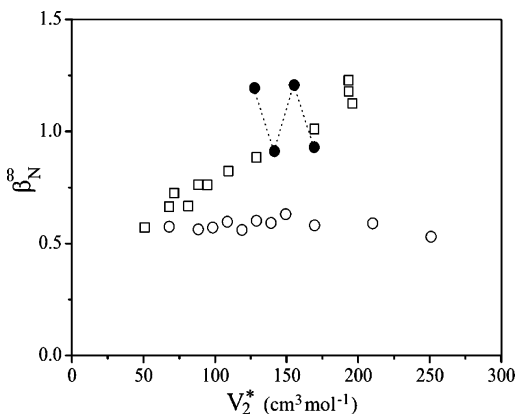


**Figure 2.** Correlation between  $\beta_N^{\alpha}$ 's and core volumes ( $V_2^*$ 's) of various compounds dissolved in MBBA: open circle (○), *n*-alkanes (in order of  $V_2^*$ , hexane, octane, nonane, decane, undecane, dodecane, tridecane, tetradecane, hexadecane, icosane, tetracosane; refs 3 and 7); open square (□), branched molecules (cyclopentane, 2,2-dimethylbutane, tetramethyltin, cyclooctane, 2,2,4-trimethylpentane, *cis*-decalin, hexamethyldisiloxane, 2,2,4,6,6-pentamethylheptane, 2,2,4,4,6,8,8-heptamethylnonane, tetrabutyllead, tetrabutyltin, decamethyltetrasiloxane; ref 3); filled circle (●), dimers-3, -4, -5, and -6 (this study).

At an early stage of our studies on LCs, the rotational isomeric state (RIS) scheme,<sup>8,9</sup> which has been applied mainly to polymers, was extended to conformational analysis of chain molecules dissolved in nematic solvents. To facilitate the analysis, the cylindrical-symmetry and single-ordering-matrix approximations were adopted. In the former, biaxiality  $S_{XX} - S_{YY}$  is neglected, and the latter means that the orientational order parameter  $S_{ZZ}$  is identical for all conformers. By this method, we analyzed  $^2\text{H}$  NMR data for *n*-alkanes<sup>10,11</sup> and ethers<sup>11–13</sup> dissolved in nematic solvents. However, the simplification tends to overestimate fractions of the extended conformers, and hence, the solutes appear to be considerably rigid.

Recently, we have improved the simulation scheme. From the shape anisotropy of solute, the  $S_{ZZ}$  and  $S_{XX} - S_{YY}$  terms are evaluated for each conformer. The maximum entropy (MaxEnt) method<sup>14</sup> is employed in the fitting procedure to derive the most probable solution from a limited amount of experimental data. Using the modified method, we have investigated orientational and conformational characteristics of *n*-alkanes,<sup>15,16</sup> 1,6-dimethoxyhexane,<sup>16</sup> and alcohols<sup>17,18</sup> dissolved in nematic LCs and successfully obtained results consistent with those obtained by other methods.<sup>19–23</sup> The simulation scheme has been further extended to lyotropic LCs of sodium octanoate/1-decanol/water<sup>24,17</sup> and sodium octanoate/1-butanol/water.<sup>18</sup>

In this study, we have treated model compounds of oligomer LCs (i.e., oligomeric models for polymer LCs with different spacer lengths; see Figure 3): monomeric models, 1-phenoxy-pentane (monomer-5) and 1-phenoxyhexane (monomer-6); dimeric models, 1,3-diphenoxypropane (dimer-3), 1,4-diphenoxybutane (dimer-4), 1,5-diphenoxypentane (dimer-5), and 1,6-diphenoxyhexane (dimer-6); tetrameric models, 1,5-bis{*p*-[5-(phenoxy)pentyl]oxy}phenoxy}pentane (tetramer-5) and 1,6-bis{*p*-[5-(phenoxy)hexyl]oxy}phenoxy}hexane (tetramer-6). In this paper, these compounds are referred to by the abbreviations in the parentheses. The benzene ring and ether chain are considered to be the mesogenic core and spacer (or tail), respectively. The abbreviations represent the number of benzene rings and carbon atoms in the ether chain: For example, tetramer-5 has four benzene rings and three ethereal spacers with five methylene units. The reasons we have adopted these model compounds are as follows: Mesogens of LCs mostly have rotatable bond(s) and polarized substituent(s). The obscuri-

ties about the geometries and dipole–dipole and electrostatic interactions may impede modeling for conformational analysis. Although the model compounds here are not LCs in the narrow sense, they are free from the above problems. Crystal-to-nematic (CN) and NI transition temperatures, enthalpies, and entropies of LCs largely depend on the spacer length (i.e., the number of atoms in the spacer chain). This phenomenon has been found for oligomer to polymer LCs and designated as the odd–even effect or odd–even oscillation.<sup>1,25–29</sup> To elucidate its origin and nature, we have adopted the oligomeric models with ether chains of different lengths.

In this study, *ab initio* molecular orbital (MO) calculations were carried out for the monomers and dimers to obtain the conformational energies for the isolated (free) states. Thermal properties of the dimers and tetramers were investigated from DSC measurements. Crystal structures of the dimeric models were determined by single-crystal X-ray diffraction. Phase behaviors of the dimer/MBBA systems were investigated at low solute concentrations to estimate the molecular shapes in the nematic solutions. The deuterated model compounds were prepared, dissolved in a nematic LC (either MBBA or PAA), and measured by  $^2\text{H}$  NMR spectroscopy. The NMR data were analyzed by our improved method to evaluate the orientational order parameters, bond conformations, and molecular dimensions; the applicability of the method to the complicated LC-like molecules has been examined. From the theoretical and experimental investigations, the liquid crystallinity of oligomer to polymer LCs as well as the model compounds is discussed here.

## 2. Materials and Methods

**2.1. *Ab Initio* MO Calculations.** *Ab initio* MO calculations were carried out for representative conformers of the monomeric and dimeric model compounds with the *Gaussian98* program<sup>30</sup> installed on an HPC-P4L/IAX computer. The geometrical parameters were fully optimized, and the thermal corrections were calculated at the Hartree–Fock (HF) level using the 6-31G(d) basis set (abbreviated as HF/6-31G(d)). Then, a scale factor of 0.9135 was used to adjust the thermodynamic quantities.<sup>31,32</sup> With the geometrical parameters determined, the single-point calculation was performed by including up to the second-order Møller–Plesset (MP2) perturbation with the 6-311+G(3df,2p) basis set (MP2/6-311+G(3df,2p)). The Gibbs free energies ( $\Delta G_k$ 's,  $k$  = conformer) were evaluated from the SCF energy and the thermal correction. In addition, geometries of some conformers were optimized at the B3LYP/6-31G(d) level to be used in simulations for  $^2\text{H}$  NMR data.

**2.2. Sample Preparation.** Here, only deuterations of the model compounds and MBBA are described;<sup>33</sup> however, the nondeuterated compounds were similarly prepared and used in measurements other than  $^2\text{H}$  NMR. Symbols *o* and *ϕ* represent the ortho and ortho + meta positions of the benzene rings, respectively. Nondeuterated MBBA and PAA were, respectively, purchased from Tokyo Kasei Kogyo and Sigma-Aldrich and used without further purification.

**2.2.1. Monomer-5-*d*<sub>11</sub>.**<sup>34</sup> Pentanoic acid (30.6 g) was dissolved in methanol (100 mL), and sodium hydroxide was added so that the pH would be 8.0. The solution was condensed, the residue was dried under reduced pressure, and sodium pentanoate (24.7 g) was obtained. The sodium pentanoate (24.7 g), sodium hydroxide (5.4 g), platinum on activated carbon (Pt/C, Pt 5%, 7.6 g), and deuterium oxide (99 atom % D, 100 mL) were sealed in a 300-mL autoclave and heated at 220 °C for 110 h. After being cooled to room temperature, the reaction

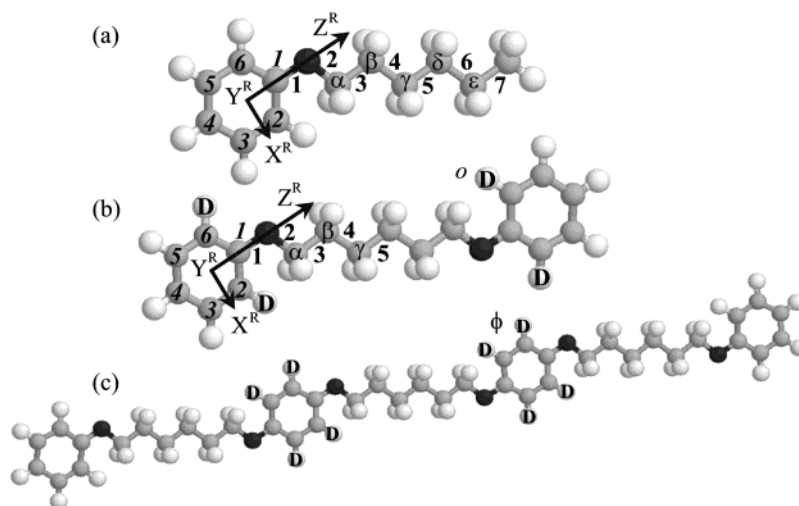


**Figure 3.** Examples of the model compounds: (a) monomer-6, (b) dimer-6, and (c) tetramer-6. The methylene and methyl groups in the ether chain are referred to by Greek letters ( $\alpha$ ,  $\beta$ ,  $\gamma$ ,  $\delta$ ,  $\epsilon$ ), and the bonds and the aromatic carbons are numbered as indicated. For the tetramers, the atomic groups and bonds are designated in the same manner as for the dimers. In tetramer-6- $d_{12}$ , only the central spacer is deuterated. The  $X^R$ ,  $Y^R$ , and  $Z^R$  axes are defined for the phenyl groups of the monomers and dimers. The ortho and ortho + meta positions of the aromatic ring are represented by  $o$  and  $\phi$ , respectively.

mixture was filtered, acidified to pH = 4 with hydrochloric acid (5.0 mol L<sup>-1</sup>), and extracted with diethyl ether. After being dried over sodium sulfate, the organic extract was filtered and condensed to yield perdeuterated pentanoic acid. The above procedures were repeated to obtain an adequate amount for the next step. The total yield was 15.7 g.

The deuterated pentanoic acid (15.7 g) was dissolved in dry THF and added dropwise to a solution of LiAlD<sub>4</sub> (10.1 g) in THF (300 mL), and the mixture was refluxed for 2 h. The residual LiAlD<sub>4</sub> was quenched with water, and Wakogel C-200 (13.0 g) was added to absorb inorganic deposits. After being stirred for 1 h, the mixture was diluted with THF (300 mL) and allowed to stand. The top clear layer was filtered with suction and condensed, and 12.3 g of 1-pentanol- $d_{11}$  was obtained.

Phosphorus tribromide (12.8 g) was added dropwise to the 1-pentanol- $d_{11}$  (12.3 g). The mixture was refluxed for 2 h, washed with water (100 mL), and filtered with suction. The filtrate separated into three layers: 1-pentanol- $d_{11}$ , water, and 1-bromopentane- $d_{11}$ . Only the bottom layer (1-bromopentane- $d_{11}$ ) was collected, then Wakogel C-200 (5.0 g) was added, and the mixture was stirred and filtered. After being dried over sodium sulfate overnight, the solution was filtered, and 10.0 g of 1-bromopentane- $d_{11}$  was obtained.

The 1-bromopentane- $d_{11}$  (10.0 g), 1-bromopentane (9.4 g), potassium hydroxide (7.1 g), and phenol (11.7 g) were dissolved in ethanol (85 mL), and the solution was refluxed for 8 h. The reaction mixture was filtered, distilled to remove ethanol, and extracted with diethyl ether (100 mL) and water (100 mL). The organic extract was washed successively with potassium hydroxide (10%), water, dilute sulfuric acid, and water again. After being dried over sodium sulfate, the solution was filtered and distilled under pressure to yield monomer-5- $d_{11}$  (1-phenoxy-pentane-1,1,2,2,3,3,4,4,5,5,5- $d_{11}$ , 7.3 g).

**2.2.2. Monomer-6- $d_{13}$ .** This compound was prepared in the same way as in section 2.2.1, except that hexanoic acid and phosphorus trichloride were used in place of pentanoic acid and phosphorus tribromide, respectively.

**2.2.3. Monomer-5- $\alpha$ - $d_2$  and Monomer-6- $\alpha$ - $d_2$ .** These partial deuterides were prepared from nondeuterated pentanoic and hexanoic acids, as described in sections 2.2.1 and 2.2.2.

**2.2.4. Phenol- $o$ - $d_2$ .** Phenol (25.0 g) was dissolved in ethanol- $d_6$  (50 g), deuterium chloride (20 wt % solution in deuterium oxide, 100 g) was added, and the solution was refluxed for 50 h. The reaction mixture was condensed to remove deuterium oxide, dried over sodium sulfate, and filtered. After the filtrate was cooled, precipitated phenol-2,6- $d_2$  (phenol- $o$ - $d_2$ , 16.5 g) was collected by suction filtration and dried under reduced pressure.

**2.2.5. Dimer-3- $d_6$ , Dimer-4- $d_8$ , Dimer-5- $d_{10}$ , and Dimer-6- $d_{12}$ .** These deuterides were prepared by procedures similar to those in section 2.2.1. Malonic, succinic, glutaric, and adipic acids were deuterated with NaOH, Pt/C, and D<sub>2</sub>O, and reduced with LiAlD<sub>4</sub> to yield 1,3-propanediol- $d_6$ , 1,4-butanediol- $d_8$ , 1,5-pentanediol- $d_{10}$ , and 1,6-hexanediol- $d_{12}$ , respectively. These diols were converted to the corresponding  $\alpha,\omega$ -dibromoalkanes with phosphorus tribromide. Dimer-3- $d_6$  (1,3-diphenoxypropane-1,1,2,2,3,3- $d_6$ ), dimer-4- $d_8$ , dimer-5- $d_{10}$ , and dimer-6- $d_{12}$  were prepared from the  $\alpha,\omega$ -dibromoalkanes and phenol. The end products were purified by recrystallization in methanol.

**2.2.6. Dimer-3- $o$ - $d_4$ , Dimer-4- $o$ - $d_4$ , Dimer-5- $o$ - $d_4$ , and Dimer-6- $o$ - $d_4$ .** As described in section 2.2.5, these compounds were prepared with the phenol- $o$ - $d_2$  obtained in section 2.2.4.

**2.2.7. Tetramer-5- $d_{10}$ .**<sup>35</sup> Phenol (2.5 g) and potassium hydroxide, dissolved in ethanol (90 mL), were added dropwise to a solution of 1,5-dibromopentane (44.0 g) in ethanol (100 mL). To avoid formation of 1,5-diphenoxypentane, 1,5-dibromopentane was used in large excess. The mixture was refluxed for 8 h, filtered, condensed, and extracted with water and diethyl ether. The organic extract was washed successively with sodium hydroxide (10%), water, dilute sulfuric acid, and water again. The solution was dried over sodium sulfate, filtered, and distilled under reduced pressure to yield 1-bromo-5-phenoxy-pentane (3.2 g).

Chlorobenzene (20 mL), hydroquinone (6.12 g), sodium hydroxide (1.67 g), and water (20 mL) were mixed, stirred into a uniform solution, and heated to 100 °C. To the mixture, 1,5-dibromopentane- $d_{10}$  (3.2 g), prepared as in section 2.2.5, was added dropwise. After reflux for 10 h, the solution was acidified with hydrochloric acid. The precipitate was collected by suction filtration and dried under pressure, and 1.8 g of 1,5-bis(*p*-hydroxyphenoxy)pentane- $d_{10}$  was obtained.

The 1,5-bis(*p*-hydroxyphenoxy)pentane-*d*<sub>10</sub> (1.3 g), 1-bromo-5-phenoxy-pentane (3.2 g), and potassium hydroxide (0.5 g) were dissolved in ethanol (100 mL) and refluxed for 10 h. Precipitated tetramer-5-*d*<sub>10</sub> was collected by suction filtration. The solubility of the product was examined to find proper solvents for recrystallization. It is slightly soluble in chloroform but insoluble in methanol, water, dimethyl sulfoxide, *n*-hexane, THF, and diethyl ether. The crude product was recrystallized with chloroform, and 2.1 g of the end product, tetramer-5-*d*<sub>10</sub> (1,5-bis{*p*-[5-(phenoxy)pentyl]oxy}phenoxy}pentane-1,1,2,2,3,3,4,4,5,5-*d*<sub>10</sub>), was obtained.

**2.2.8. Tetramer-6-*d*<sub>12</sub>.** This compound was prepared as in section 2.2.7, except that 1,6-dibromohexane was used instead of 1,5-dibromopentane.

**2.2.9. Tetramer-5-*φ*-*d*<sub>8</sub> and Tetramer-6-*φ*-*d*<sub>8</sub>.** Hydroquinone (27.2 g) was dissolved in deuterium oxide (100 mL). Sulfuric acid-*d*<sub>2</sub> (3.4 g) was added dropwise, and the solution was refluxed for 5 days. After the reaction mixture was cooled in a refrigerator, the precipitate was collected by suction filtration, and 19.7 g of perdeuterated hydroquinone was obtained. Tetramer-5-*φ*-*d*<sub>8</sub> and tetramer-6-*φ*-*d*<sub>8</sub> were prepared with the hydroquinone-*d*<sub>6</sub>, as in section 2.2.7.

**2.2.10. MBBA-2,6-*d*<sub>2</sub>.** This compound was prepared from *p*-anisaldehyde and *p*-butylaniline-2,6-*d*<sub>2</sub> as described previously.<sup>11,36</sup>

**2.3. <sup>2</sup>H NMR Measurements.** The required amounts of the model compound (solute) and nematic solvent (MBBA or PAA) were weighed in a standard NMR tube of 5 mm o.d. The sample tube was degassed, filled with dry nitrogen, and sealed to avoid thermal degradation of the solvent by oxygen.

Deuterium NMR spectra were recorded at 76.65 MHz on a JEOL JNM LA-500 spectrometer equipped with a variable-temperature controller. During the measurement, the probe temperature was maintained at a given temperature within ±0.1 °C fluctuations. The free induction decays (FIDs) were accumulated 256–2048 times by using the single pulse excitation scheme. The  $\pi/2$  pulse width was so determined as to maximize the signal-to-noise ratio as 15  $\mu$ s for the monomers and dimers or 20  $\mu$ s for the tetramers, and the recycle delay was 1.0 s. The FID underwent Fourier transformation by the *gNMR* program.<sup>37</sup> In the apodization, an exponential function was used; the broadening factor was set to 5–20 Hz.

**2.4. Thermal Analysis.** Thermal analyses were carried out for the dimers and tetramers with a Rigaku DSC8230 differential scanning calorimeter at a heating rate of 5 °C min<sup>-1</sup> under a flow of dry nitrogen. The melting points and enthalpies of fusion were calibrated from those of indium, tin, and lead of high purity.

**2.5. X-ray Diffraction.** Single crystals of dimers-3, -4, -5, and -6 were prepared by recrystallization at room temperature from the 1-butanol, *n*-hexane, 1-butanol, and methanol solutions, respectively. It took several days to a few weeks for the crystals to grow large and thick enough (ca. 0.4 × 0.4 × 0.2 mm<sup>3</sup>) for X-ray measurements. Dimers-3 and -5 yielded colorless needle crystals, and dimers-4 and -6 gave colorless plate crystals. The latter crystallized faster than the former.

The X-ray diffraction was measured with a Bruker SMART-1000 CCD system, and monochromatic Mo K $\alpha$  radiation was generated at 45 kV and 35 mA. The single crystal was mounted on a glass fiber and cooled to a low temperature. Reflection intensities were collected to a maximum  $2\theta$  value of ca. 57° with 0.60° oscillations and 20 s exposures. The crystal-to-detector distance was 50 mm. All crystallographic computations

were performed using the *teXsan* crystallographic software package.<sup>38</sup>

Crystal data on dimer-3: C<sub>15</sub>H<sub>16</sub>O<sub>2</sub>, monoclinic crystal system, space group *C2/c*,  $a = 21.697(7)$  Å,  $b = 5.134(2)$  Å,  $c = 11.2054$  Å,  $\beta = 99.721(4)^\circ$ ,  $V = 1230.3(6)$  Å<sup>3</sup>,  $Z = 4$ ,  $\rho_{\text{calc}} = 1.232$  g cm<sup>-3</sup>, data collection at -100 °C, residual  $R = 0.088$ . Crystal data on dimer-4: C<sub>16</sub>H<sub>18</sub>O<sub>2</sub>, monoclinic crystal system, space group *P2<sub>1</sub>/c*,  $a = 14.883(3)$  Å,  $b = 5.541(1)$  Å,  $c = 7.966(2)$  Å,  $\beta = 99.759(3)^\circ$ ,  $V = 647.3(2)$  Å<sup>3</sup>,  $Z = 2$ ,  $\rho_{\text{calc}} = 1.243$  g cm<sup>-3</sup>, data collection at -110 °C, residual  $R = 0.062$ . Crystal data on dimer-5: C<sub>17</sub>H<sub>20</sub>O<sub>2</sub>, monoclinic crystal system, space group *C2/c*,  $a = 26.042(8)$  Å,  $b = 5.110(2)$  Å,  $c = 11.162(3)$  Å,  $\beta = 107.019(4)^\circ$ ,  $V = 1420.3(7)$  Å<sup>3</sup>,  $Z = 4$ ,  $\rho_{\text{calc}} = 1.199$  g cm<sup>-3</sup>, data collection at -100 °C, residual  $R = 0.075$ . Crystal data on dimer-6: C<sub>18</sub>H<sub>22</sub>O<sub>2</sub>, monoclinic crystal system, space group *P2<sub>1</sub>/c*,  $a = 15.835(5)$  Å,  $b = 7.133(2)$  Å,  $c = 6.534(2)$  Å,  $\beta = 92.143(4)^\circ$ ,  $V = 737.6(4)$  Å<sup>3</sup>,  $Z = 2$ ,  $\rho_{\text{calc}} = 1.217$  g cm<sup>-3</sup>, data collection at -153 °C, residual  $R = 0.073$ .

**2.6. Phase Behavior Observations.** The procedure for the sample preparation and measurement has been described previously.<sup>11,18</sup>

### 3. Results and Discussion

**3.1. Ab Initio MO Calculations and Conformational Free Energies.** According to the RIS scheme,<sup>8,9</sup> statistical weight matrices for bonds 2 and  $n$  ( $n \geq 3$ ) (see Figure 3) of the ether chains of the monomers, dimers, and tetramers may be written as

$$U_2 = \begin{bmatrix} 1 & \sigma_2 & \sigma_2 \\ 0 & 0 & 0 \\ 0 & 0 & 0 \end{bmatrix} \quad (1)$$

and

$$U_n = \begin{bmatrix} 1 & \sigma_n & \sigma_n \\ 1 & \sigma_n & \sigma_n \omega_n \\ 1 & \sigma_n \omega_n & \sigma_n \end{bmatrix} \quad (2)$$

where  $\sigma_n$  is the statistical weight for the first-order interaction (between atoms and groups separated by three bonds) of bond  $n$ , and  $\omega_n$  is the second-order interaction (by four bonds) occurring in  $g^\pm g^\mp$  conformations for bonds  $n - 1$  and  $n$ . The statistical weight is the Boltzmann factor of the corresponding conformation energy (e.g.,  $\sigma_n = \exp(-E_{\sigma n}/RT)$ , where  $R$  is the gas constant and  $T$  is the absolute temperature). Both MO calculations and X-ray diffraction indicate that the phenyl C<sub>1</sub>-C<sub>2</sub> and ethereal O-C $\alpha$  bonds are fixed in an eclipsed form; therefore, the internal rotation of bond 1 has not been considered (see Figure 3).

In the RIS scheme, the  $\Delta G_k$  value relative to the all-trans state is approximated as a function of  $E_\sigma$ 's and  $E_\omega$ 's. For example, the  $g^+tt\dots$ ,  $tg^+t\dots$ , and  $ttg^+\dots$  conformations have weights of  $\sigma_2$ ,  $\sigma_3$ , and  $\sigma_4$ , respectively; therefore, the individual  $\Delta G_k$  values may correspond to  $E_{\sigma_2}$ ,  $E_{\sigma_3}$ , and  $E_{\sigma_4}$ , respectively. Here, for example, the  $g^+tt\dots$  conformation represents that bonds 2, 3, 4... adopt gauche<sup>+</sup>, trans, trans... states, respectively. The  $tg^+g^-\dots$  conformation has a weight of  $\sigma_3\sigma_4\omega_4$ . Thus, the  $E_{\omega_4}$  value may be obtained from  $\Delta G_{tg^+g^-\dots} - E_{\sigma_3} - E_{\sigma_4}$ . Similarly, all  $E_\sigma$  and  $E_\omega$  values of the monomers and dimers were evaluated from  $\Delta G_k$ 's at the MP2/6-311+G(3df,2p)/HF/6-31G(d) level, as shown in Table 1.

The  $E_{\sigma_n}$  value corresponds to the gauche energy. In the C-O bond, the trans conformation is stable ( $E_{\sigma_2} \approx 1$  kcal mol<sup>-1</sup>), whereas its adjoining C-C bond shows a gauche preference

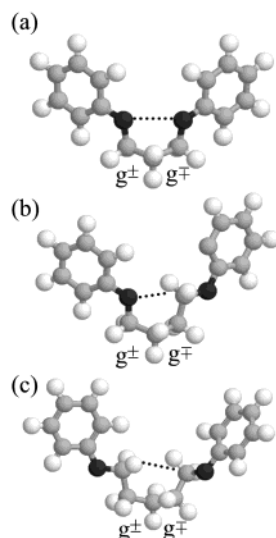


**Figure 4.** Examples of second-order  $\omega_n$  interactions occurring in the  $g^+g^-$  conformations for the  $n - 1$  and  $n$  bond pairs: (a)  $\omega_4$  of dimer-3, (b)  $\omega_4$  of dimer-4, and (c)  $\omega_5$  of dimer-5.

**TABLE 1: Conformational Energies of Monomeric and Dimeric Model Compounds, Evaluated from ab Initio MO Calculations at MP2/6-311+G(3df, 2p)//HF/6-31G(d) Level<sup>a</sup>**

	monomer-5	monomer-6	dimer-3	dimer-4	dimer-5	dimer-6
First-Order Interaction						
$E_{\sigma_2}$	0.91	0.90	0.94	1.13	0.86	0.89
$E_{\sigma_3}$	-0.31	-0.33	-1.18	-0.30	-0.61	-0.39
$E_{\sigma_4}$	0.65	0.61		0.69	0.49	0.65
$E_{\sigma_5}$	0.59	0.59				0.52
$E_{\sigma_6}$		0.63				
Second-Order Interaction						
$E_{\omega_4}$	0.45	0.43	2.62	-0.66	0.52	0.13
$E_{\omega_5}$	1.55	1.40			1.35	1.34
$E_{\omega_6}$		1.71				

<sup>a</sup> In kcal mol<sup>-1</sup>.

( $E_{\sigma_3} = -0.3$  to  $-1.2$  kcal mol<sup>-1</sup>), which is known as the attractive gauche effect in X-C-C-Y bond sequences (X, Y = electronegative atoms).<sup>39,40</sup> The  $E_{\sigma}$  values (0.5–0.7 kcal mol<sup>-1</sup>) for other C-C bonds are essentially equivalent to that ( $\sim 0.5$  kcal mol<sup>-1</sup>) of *n*-alkanes.<sup>8,41</sup> The  $E_{\omega_n}$  value represents the additional energy occurring in the  $g^+g^-$  conformations for bonds  $n - 1$  and  $n$ . In bonds 2 and 3, the  $\omega_3$  conformation does not exist because of a steric conflict between the benzene ring and  $\gamma$  methylene group; therefore, the  $E_{\omega_3}$  value has been assumed to be  $\infty$ , being absent from Table 1. For the dimers, the magnitude of  $E_{\omega_4}$  depends on the number of methylene units in the spacer. Dimer-3 exhibits a large positive value of 2.62 kcal mol<sup>-1</sup> due to the O...O repulsion (Figure 4a). On the other hand, dimer-4 gives a negative value of  $-0.66$  kcal mol<sup>-1</sup>. This is due to the (C-H)...O attraction between the oxygen and the  $\alpha$  methylene group (Figure 4b). This phenomenon has also been found in poly(ethylene oxide),<sup>42–45</sup> poly(propylene oxide),<sup>45–48</sup> poly(tetramethylene oxide),<sup>47,49</sup> and their model compounds. Dimers-5 and -6 have small positive  $E_{\omega_4}$  values of 0.52 and 0.13 kcal mol<sup>-1</sup>, respectively. A similar variation in  $E_{\omega}$  with the number of methylene units has been found for  $\alpha,\omega$ -dimethoxyalkanes CH<sub>3</sub>O(CH<sub>2</sub>)<sub>x</sub>OCH<sub>3</sub> ( $x = 4–8$ ); the  $E_{\omega}$  values for  $x = 4, 5,$  and  $6$  were evaluated from ab initio MO calculations at the MP2/6-31+G\*//HF/6-31G\* level to be  $-0.43, 0.66,$  and  $0.24$  kcal mol<sup>-1</sup>, respectively.<sup>49</sup> The  $\omega_5$  and  $\omega_6$  interactions correspond to the so-called pentane effect (Figure 4c); however, the  $E_{\omega_5}$  and  $E_{\omega_6}$  values (1.3–1.7 kcal mol<sup>-1</sup>) are

**TABLE 2: Melting Points ( $T_M$ 's) and Enthalpies ( $\Delta H_M$ 's) and Entropies ( $\Delta S_M$ 's) of Fusion of Dimeric and Tetrameric Model Compounds**

	$T_M$ (°C)	$\Delta H_M$ (kJ mol <sup>-1</sup> )	$\Delta S_M$ (J mol <sup>-1</sup> K <sup>-1</sup> )
dimer-3	59.1	38.3	115
dimer-4	98.0	54.6	147
dimer-5	44.1	41.8	132
dimer-6	80.5	56.0	158
tetramer-5 <sup>a</sup>	77.3	39.0	111
	99.3	83.4	224
tetramer-6	143.7	166.2	399

<sup>a</sup> On heating, two endothermic peaks were observed.

smaller than that (2–3 kcal mol<sup>-1</sup>) of *n*-alkanes.<sup>8,41</sup> These energy parameters represent the inherent conformational features of the model compounds in the isolated (free) state. One should be allowed to assume that the central spacers of tetramers-5 and -6 have essentially the same conformational energies as those of dimers-5 and -6, respectively.

**3.2. Thermal Analysis.** In Table 2, DSC data for the dimers and tetramers are listed. Melting points ( $T_M$ 's) and enthalpies ( $\Delta H_M$ 's) and entropies ( $\Delta S_M$ 's) of fusion of the dimers show clear odd–even oscillations: Dimers-4 and -6 exhibit larger values than dimers-3 and -5. As mentioned in the Introduction, similar phenomena have been found for oligomer to polymer LCs. For example, CBA-*x*'s exhibit CN and NI transitions.<sup>25</sup> The sums of both transition enthalpies for  $x = 3, 4, 5,$  and  $6$ , equivalent to the enthalpy of fusion, were evaluated as 47.5, 50.2, 32.7, and 55.8 kJ mol<sup>-1</sup>, close to those obtained here for the dimers.

Tetramer-5 undergoes two transitions to the melting point: the first occurring at 77.3 °C is probably a crystal-to-crystal transition, and the second at 99.3 °C is the actual melting point. The sum of the two transition enthalpies is 122.4 kJ mol<sup>-1</sup>. Tetramer-6 melts at 143.7 °C, and the enthalpy of fusion is 166.2 kJ mol<sup>-1</sup>. Because the tetramers have three spacers, enthalpies per spacer of tetramers-5 and 6 are, respectively, 40.8 and 55.4 kJ mol<sup>-1</sup>, almost the same as those of dimers-5 and -6.

**3.3. Crystal Structures of Dimers.** Figure 5 shows crystal structures of the four dimers, and the individual molecules are depicted in Figure 6. The molecules of dimers-3 and -5 are bent at right angles; angles ( $\theta$ 's) between para axes of the two phenyl rings (see Figure 7) are 86.6° (dimer-3) and 85.8° (dimer-5). The two C-C bonds adjacent to the C-O bond adopt the  $g^-$  conformation. Accordingly, dimers-3 and -5 crystallize to be in one of the most stable states predicted by the MO calculations.

Dimer-4 forms an effective intermolecular stacking arrangement of the phenyl rings. Its spacer adopts a stable  $tg^+tg^-t$  conformation, which yields a parallel arrangement of the two phenyl groups ( $\theta = 0.0^\circ$ ). These facts suggest that dimer-4 forms a thermally stable crystal. The molecules of dimer-6 are arranged parallel to each other but are forced to be in the all-trans state ( $\theta = 0.0^\circ$ ), despite the gauche preference of bond 3 ( $E_{\sigma_3} = -0.39$  kcal mol<sup>-1</sup>).

The odd–even effect in the crystal structure corresponds to the effect in the thermal properties. Dimers-4 and -6 can attain the parallel molecular arrangement and effective benzene stacking and, hence, give larger  $\Delta H_M$  values than dimers-3 and -5. Crystal densities of dimers-3, -4, -5, and -6 are 1.232, 1.243, 1.199, and 1.217 g cm<sup>-3</sup>, respectively. The  $\Delta S_M$  values of tetramers-5 and -6 are 335 (= 111 + 224) and 399 J mol<sup>-1</sup> K<sup>-1</sup>, respectively. From these data, their entropies per spacer can be estimated as 112 (tetramer-5) and 133 (tetramer-6) J mol<sup>-1</sup> K<sup>-1</sup>, comparable to those of dimers-5 and -6, respectively.

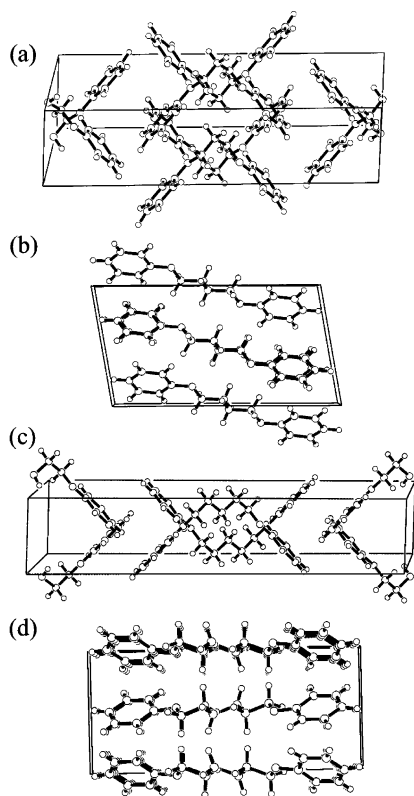


**Figure 5.** Crystal structures of (a) dimer-3, (b) dimer-4, (c) dimer-5, and (d) dimer-6. For the details, see section 2.5.

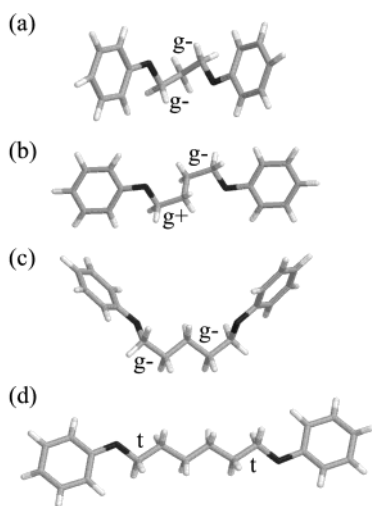


**Figure 6.** Molecules in the crystal: (a) dimer-3, (b) dimer-4, (c) dimer-5, and (d) dimer-6. The conformations of the C–C bonds adjacent to the ether linkage are shown.

In the crystal, therefore, tetramers-5 and -6 may be similar in spacer conformation to dimers-5 and -6, respectively.

**3.4. Phase Behaviors of Dimers.** In Figure 8, as an example, the phase diagram of the dimer-3/MBBA system is shown. The filled circles and squares represent the experimental data. Linear least-squares fitting to the lower and upper boundaries yielded the slopes of 1.269 ( $\beta_N$ ) and 0.993 ( $\beta_I$ ), respectively. The slopes at the infinite dilution,  $\beta_N^\infty$  and  $\beta_I^\infty$ , can be evaluated from the  $\beta_N$  and  $\beta_I$  values, as in previous papers:<sup>3–7,11,18</sup> dimer-3/MBBA,  $\beta_N^\infty = 1.194$  and  $\beta_I^\infty = 1.059$ ; dimer-4/MBBA,  $\beta_N^\infty = 0.912$  and  $\beta_I^\infty = 0.831$ ; dimer-5/MBBA,  $\beta_N^\infty = 1.207$  and  $\beta_I^\infty = 1.069$ ; dimer-6/MBBA,  $\beta_N^\infty = 0.930$  and  $\beta_I^\infty = 0.846$ . In Figure 2, the

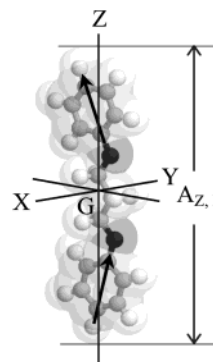


**Figure 7.** Molecular axis system for, for example, dimer-3. The origin is located at the center of gravity,  $G$ . The principal axes of inertia are assumed to be the molecular axes,  $X$ ,  $Y$ , and  $Z$ . The dimension along the  $Z$  axis,  $A_{Z,k}$ , calculated from the van der Waals radii of the constituent atoms, is considered to be the conformer length. The angle between two para-axis vectors (shown by the arrows) of the phenoxy groups is designated as  $\theta$ .

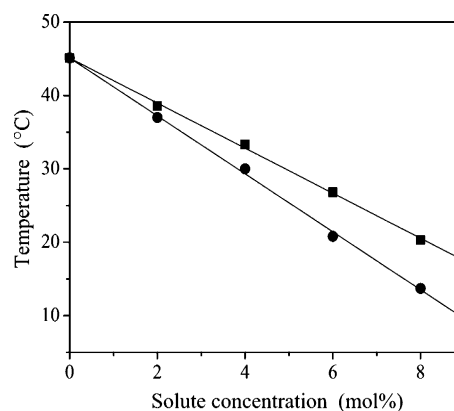


**Figure 8.** Phase diagram of the dimer-3/MBBA system. Slopes of the upper ( $\beta_I$ ) and lower ( $\beta_N$ ) boundaries were determined as 0.993 and 1.269, respectively, on the scale of  $T/T_{NI}$  versus mole fraction. Here,  $T_{NI}$  stands for the NI transition temperature of pure MBBA.

$\beta_N^\infty$  values are plotted against the core volume  $V_2^*$  of the solute.<sup>50</sup>

If two solutes have the same  $V_2^*$  value, the one with a larger  $\beta_N^\infty$  is expected to be more globular than the other. The  $\beta_N^\infty$  values for the dimer/MBBA systems are plotted with filled circles in Figure 2. The four points, showing a large odd–even oscillation, are located in the region of spherical solutes. In the nematic LC, the dimers are spherical rather than linear, and dimers-3 and -5 are more isotropic in shape than dimers-4 and -6.

**3.5.  $^2\text{H}$  NMR Spectra.** **3.5.1. Monomers.** Panels a and b of Figure 9 show  $^2\text{H}$  NMR spectra observed from monomer-5- $d_{11}$  and monomer-5- $d_{11}$  + monomer-5- $\alpha$ - $d_2$  dissolved in MBBA at 25 °C and 2.0 mol % (of solute), respectively. By a comparison of the two spectra, we could assign the second peaks from the outside to the  $\alpha$  methylene group. The interpeak distance corresponds to the quadrupolar splitting ( $|\Delta\nu_\alpha|$ ). The other quadrupolar splittings were so assigned as to decrease in the order of the Greek alphabet. Figure 9c shows a  $^2\text{H}$  NMR spectrum of monomer-6- $d_{13}$  in MBBA at 25 °C and 2.0 mol %. Similarly, the quadrupolar splittings were assigned as shown in Figure 9.<sup>52</sup> The  $|\Delta\nu|$  values are given in the caption of Figure 9.

**3.5.2. Dimers.** Panels a and b of Figure 10 show  $^2\text{H}$  NMR spectra of dimer-3- $d_6$  + dimer-3- $o$ - $d_2$  and dimer-4- $d_8$  + dimer-4- $o$ - $d_2$  dissolved in MBBA at 25 °C and 2.0 mol %, respectively.

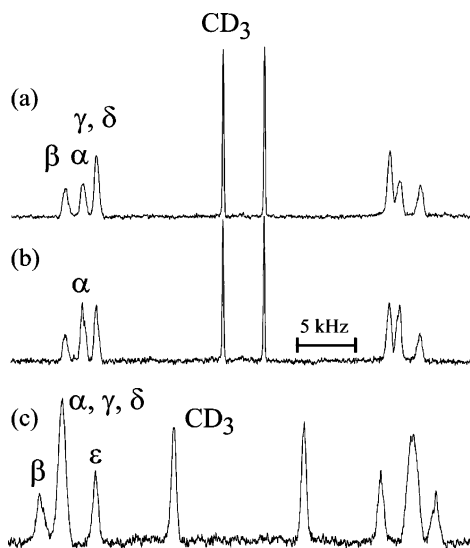


**Figure 9.** Deuterium NMR spectra observed from (a) monomer-5- $d_{11}$ , (b) monomer-5- $d_{11}$  + monomer-5- $\alpha$ - $d_2$ , and (c) monomer-6- $d_{13}$  dissolved in MBBA at 25 °C and 2.0 mol % (of solute), respectively. As indicated, the peaks were assigned to the individual atomic groups (see Figure 3). The  $|\Delta\nu|$  values of the  $\alpha$ ,  $\beta$ ,  $\gamma$ , and  $\delta$  methylene and methyl groups of monomer-5- $d_{11}$  are, respectively, 27.30, 30.55, 25.27, 25.27, and 3.55 kHz, and those of the  $\alpha$ ,  $\beta$ ,  $\gamma$ ,  $\delta$ , and  $\epsilon$  methylene and methyl groups of monomer-6- $d_{13}$  are respectively 31.35, 35.44, 31.35, 31.35, 25.52, and 11.63 kHz.

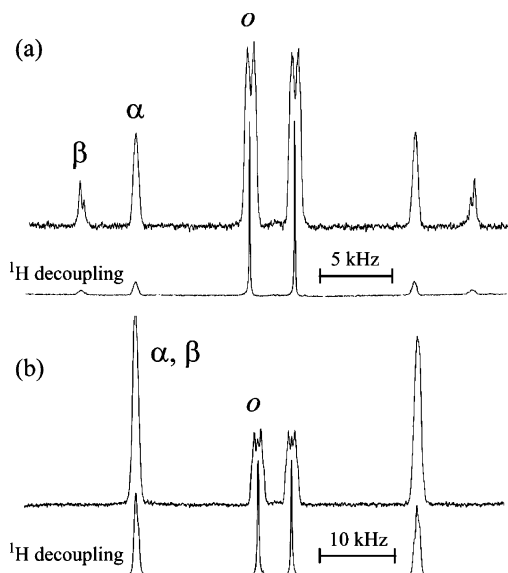


**Figure 10.** Deuterium NMR spectra observed from (a) dimer-3- $d_6$  + dimer-3- $o$ - $d_2$  and (b) dimer-4- $d_8$  + dimer-4- $o$ - $d_2$  dissolved in MBBA at 25 °C and 2.0 mol %. As indicated, the peaks were assigned to the individual atomic groups. The  $|\Delta\nu|$  values of the  $\alpha$  and  $\beta$  methylene groups and the ortho C–D bond are, respectively, 19.56, 27.31, and 3.11 kHz (dimer-3); and 35.64, 35.64, and 4.31 kHz (dimer-4). The  $|D_{HD}|$  values of dimers-3 and -4 are 230 and 410 Hz, respectively.

The upper and lower spectra were measured without and with  $^1\text{H}$  broad-band decoupling, respectively. Dimer-3 has two  $\alpha$  and one  $\beta$  methylene units; the former peaks must be more intense than the latter peaks. Therefore, the outermost and second pairs of peaks were assigned to the  $\beta$  and  $\alpha$  methylene groups, respectively. The two innermost doublets come from the ortho C–D bonds of the phenyl ring. The doublet is due to dipolar coupling ( $D_{HD}$ ) between the ortho D and meta H, and the spacing corresponds to  $2|D_{HD}|$ . For dimer-4, signals from the  $\alpha$  and  $\beta$  methylene groups overlap and form a single pair of intense peaks.

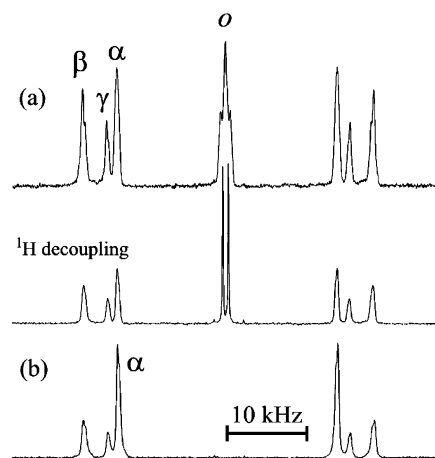


**Figure 11.** Deuterium NMR spectra observed from (a) dimer-5- $d_{10}$  + dimer-5- $o$ - $d_2$  and (b) dimer-5- $d_{10}$  + dimer-5- $\alpha$ - $d_2$  dissolved in MBBA at 25 °C and 2.0 mol %. As indicated, the peaks were assigned to the individual atomic groups. The  $|\Delta\nu|$  values of the  $\alpha$ ,  $\beta$ , and  $\gamma$  methylene groups and the ortho C–D bond are, respectively, 27.74, 36.31, 30.64, and 0.62 kHz. The  $|D_{HD}|$  value is 310 Hz.

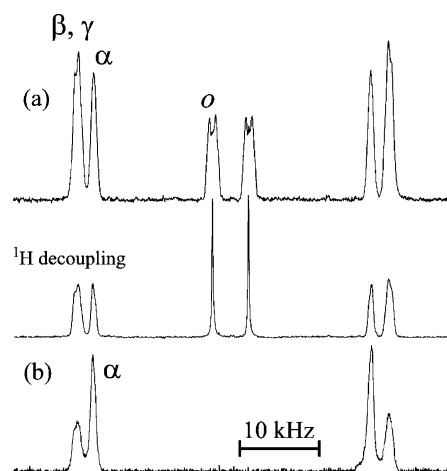


**Figure 12.** Deuterium NMR spectra observed from (a) dimer-6- $d_{12}$  + dimer-6- $o$ - $d_2$  and (b) dimer-6- $d_{12}$  + dimer-6- $\alpha$ - $d_2$  dissolved in MBBA at 25 °C and 2.0 mol %. As indicated, the peaks were assigned to the individual atomic groups. The  $|\Delta\nu|$  values of the  $\alpha$ ,  $\beta$ , and  $\gamma$  methylene groups and the ortho C–D bond are, respectively, 35.67, 40.74, 39.83, and 4.68 kHz. The  $|D_{HD}|$  value is 390 Hz.

Shown in Figure 11 are  $^2\text{H}$  NMR spectra of deuterated dimer-5 species dissolved in MBBA at 25 °C and 2.0 mol %: (a) dimer-5- $d_{10}$  + dimer-5- $o$ - $d_2$  without (upper) and with (lower)  $^1\text{H}$  broad-band decoupling and (b) dimer-5- $d_{10}$  + dimer-5- $\alpha$ - $d_2$ . Comparison of these spectra enabled us to assign the third peaks from the outside to the  $\alpha$  methylene group. Dimer-5 has two  $\alpha$ , two  $\beta$ , and one  $\gamma$  methylene units; therefore, the outermost and the smallest peaks stem from the  $\beta$  and  $\gamma$  methylene groups, respectively. The quadrupolar splitting due to the ortho C–D bond is so small that two H–D dipolar doublets overlap and appear to be a triplet.

Figure 12 shows  $^2\text{H}$  NMR spectra of deuterated dimer-6 species in MBBA at 25 °C and 2.0 mol %: (a) dimer-6- $d_{12}$  + dimer-6- $o$ - $d_2$  without (upper) and with (lower)  $^1\text{H}$  broad-band decoupling and (b) dimer-6- $d_{12}$  + dimer-6- $\alpha$ - $d_2$ . By a comparison of the spectra, we could assign the second peaks to the  $\alpha$  methylene group. The outer peaks are larger and, hence, include signals from the  $\beta$  and  $\gamma$  methylene groups. The  $|\Delta\nu|$  and  $|D_{HD}|$  values for the four dimers are given in the individual figure captions.

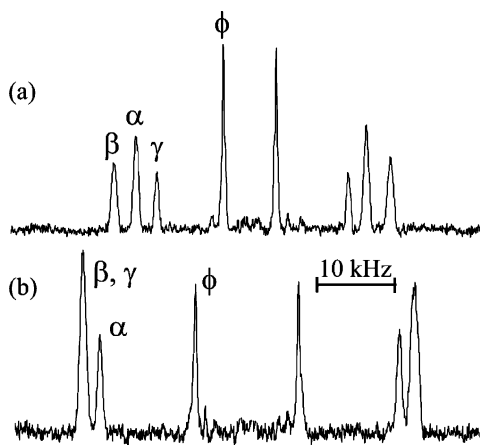


**Figure 13.** Deuterium NMR spectra observed from (a) tetramer-5- $d_{10}$  + tetramer-5- $\phi$ - $d_8$  and (b) tetramer-6- $d_{12}$  + tetramer-6- $\phi$ - $d_8$  dissolved in PAA at 120 °C and 2.0 mol %. As indicated, the peaks were assigned to the individual atomic groups. The  $|\Delta\nu|$  values of the  $\alpha$ ,  $\beta$ ,  $\gamma$  methylene groups and the phenylene C–D bond are, respectively, 27.96, 33.59, 23.26, and 6.43 kHz (tetramer-5); and 36.34, 40.25, 40.25, and 12.49 kHz (tetramer-6).

**3.5.3. Tetramers.** Figure 13 shows  $^2\text{H}$  NMR spectra of (a) tetramer-5- $d_{10}$  + tetramer-5- $\phi$ - $d_4$  and (b) tetramer-6- $d_{12}$  + tetramer-6- $\phi$ - $d_4$  dissolved in PAA at 120 °C and 2.0 mol %. The tetramers are insoluble in MBBA but slightly soluble in PAA. Thus, PAA has been used as the nematic solvent.

Intensity ratios of the outer to inner peaks of tetramer-5 are approximately 1.5:2.0:1.0:1.9. Tetramer-5 has two  $\alpha$ , two  $\beta$ , and one  $\gamma$  methylene groups. Thus, the smallest (third) peaks from the outside may come from the  $\gamma$  methylene group. The deuteration grade must be highest in the  $\alpha$  methylene group, which was generated by reduction with  $\text{LiAlD}_4$  (98 atom % D). The  $\beta$  and  $\gamma$  methylene units underwent a replacement reaction with  $\text{D}_2\text{O}$  under Pt/C. The outermost peaks may be assigned to the  $\beta$  methylene unit, because all of the monomers and dimers exhibit the largest quadrupolar splitting in the  $\beta$  methylene group. On these grounds, all of the peaks were assigned as shown in Figure 13. The eight deuteriums in the two phenylene rings (see Figure 3c), yielding only a single splitting, are essentially equivalent. Two notable differences can be found between the spectra of tetramer-5 and dimer-5: The  $\alpha$  and  $\gamma$  signals appear in reverse order, and tetramer-5 gives a much larger  $|\Delta\nu_\phi|$  than dimer-5. Because tetramer-6 gave a spectrum analogous to that of dimer-6, the assignment was carried out in a similar manner for dimer-6.

**3.6. Simulation for Quadrupolar Splittings.** **3.6.1. Procedure for Analysis.** Deuterium quadrupolar splitting  $\Delta\nu_i$  from the C–D bond at atomic group  $i$  ( $i = \alpha, \beta, \gamma, \delta, \epsilon, \text{CD}_3, o, \phi$ ) is given by

$$\Delta\nu_i = \sum_k^K \Delta\nu_{i,k} f_k \quad (3)$$

where  $K$  is the number of conformers and  $f_k$  is the fraction of conformer  $k$ . The quadrupolar splitting from the conformer,  $\Delta\nu_{i,k}$ , is expressed as<sup>53</sup>

$$\Delta\nu_{i,k} = \frac{3}{2} \frac{e^2 q Q}{h} \left[ S_{ZZ_k} \frac{3 \cos^2 \theta_{Z,i,k} - 1}{2} + (S_{XX_k} - S_{YY_k}) \frac{\cos^2 \theta_{X,i,k} - \cos^2 \theta_{Y,i,k}}{2} \right] \quad (4)$$

where  $e^2 q Q/h$  is the quadrupolar coupling constant (equal to 163 kHz for aliphatic C–D bond<sup>54</sup> or 186 kHz for aromatic C–D bond<sup>55</sup>); the  $X$ ,  $Y$ , and  $Z$  axes are the principal axes of the order matrix;  $S_{ZZ_k}$  and  $S_{XX_k} - S_{YY_k}$  are the order parameters of the conformer; and, for example,  $\theta_{X,i,k}$  is the angle between the  $X$  axis and the  $\text{C}_i$ –D bond. The  $X$ ,  $Y$ , and  $Z$  axes are assumed to be coincident with the principal axes of inertia (see Figure 7),<sup>56,57</sup> whose directions are calculated with the atomic weights located at the nuclei. The order parameter  $S_{ZZ_k}$  of conformer  $k$  is assumed to be given by<sup>58</sup>

$$S_{ZZ_k} = C(T,c) \left( \frac{a_{Z_k}}{a_{X_k} + a_{Y_k}} - \frac{1}{2} \right) \quad (5)$$

where  $C(T,c)$  is a measure of the solute–solvent interaction as a function of temperature  $T$  and solute concentration  $c$ . The biaxiality is calculated from

$$S_{XX_k} - S_{YY_k} = \frac{a_{X_k} - a_{Y_k}}{a_{Z_k}} S_{ZZ_k} \quad (6)$$

Here,  $a_{\alpha_k}$  is a semiaxis obtained from the principal moments of inertia,  $I_{\alpha\alpha_k}$ ,  $I_{\beta\beta_k}$ , and  $I_{\gamma\gamma_k}$  ( $\alpha, \beta$ , and  $\gamma = X, Y$ , and  $Z$ , respectively;  $a_{Z_k} \geq a_{X_k} \geq a_{Y_k}$ ):

$$a_{\alpha_k} = \left( \frac{5 I_{\beta\beta_k} + I_{\gamma\gamma_k} - I_{\alpha\alpha_k}}{2M} \right)^{1/2} \quad (7)$$

where  $M$  is the molecular weight.

The dipolar coupling between proton and deuteron,  $D_{\text{HD}}$ , can be calculated by substituting  $D_{\text{HD},k}$  given below for  $\Delta\nu_{i,k}$  in eq 3:<sup>53,59</sup>

$$D_{\text{HD},k} = - \frac{\gamma_{\text{H}} \gamma_{\text{D}} \hbar}{2\pi r_{\text{HD}}^3} \left[ S_{ZZ_k} \frac{3 \cos^2 \theta_{Z,\text{HD},k} - 1}{2} + (S_{XX_k} - S_{YY_k}) \frac{\cos^2 \theta_{X,\text{HD},k} - \cos^2 \theta_{Y,\text{HD},k}}{2} \right] \quad (8)$$

where  $\gamma_{\text{H}}$  and  $\gamma_{\text{D}}$  are gyromagnetic ratios of proton and deuteron, respectively,  $r_{\text{HD}}$  is the proton–deuteron distance, and  $\theta_{\alpha,\text{HD},k}$  is the angle between the  $\alpha$  axis and  $\mathbf{r}_{\text{HD}}$  vector.

The maximum entropy (MaxEnt) method has been used to derive the most reliable results from a restricted amount of experimental data.<sup>60</sup> The conformer fractions must reproduce the experimental observations. Agreement between theory and experiment may be monitored by

$$\chi^2 = \sum_i \frac{(\Delta\nu_{i,\text{calcd}} - \Delta\nu_{i,\text{obsd}})^2}{\epsilon_i^2} \quad (9)$$

where  $\Delta\nu_{i,\text{calcd}}$  and  $\Delta\nu_{i,\text{obsd}}$  are the calculated and observed quadrupolar splittings, respectively, and  $\epsilon_i$  is the experimental error.

The entropy of conformer fractions is defined as<sup>14</sup>

$$S(f_k) = \sum_{k=1}^K \left( f_k - m_k - f_k \ln \frac{f_k}{m_k} \right) \quad (10)$$

where  $m_k$  is the initial model of  $f_k$ . The MaxEnt method hypothesizes that the most probable solution of  $f_k$ 's maximizes

**TABLE 3: Bond Lengths and Bond Angles of Model Compounds<sup>a</sup>**

bond length	Å	bond angle	deg
Aromatic Ring <sup>b</sup>			
C–C	1.397	∠CCC	120.0
C–H	1.086	∠CCH	120.0
C <sub>1</sub> –O	1.367	∠C <sub>2</sub> C <sub>1</sub> O	124.6
Ether Chain <sup>c</sup>			
O–C	1.425	∠OC <sub>α</sub> H	110.0
C–C	1.530	∠CCH	109.1
C–H	1.099	∠C <sub>1</sub> OC <sub>α</sub>	118.8
		∠OC <sub>α</sub> C <sub>β</sub>	107.7
		∠CCC	112.8

<sup>a</sup> Determined from ab initio MO calculations at the B3LYP/6-31G(d) level. For the atom numbers and labels, see Figure 3. <sup>b</sup> The benzene ring is assumed to be a regular hexagon. The aromatic carbons and hydrogens and the ethereal O and C<sub>α</sub> atoms are located on the same plane. <sup>c</sup> C<sub>3</sub> symmetry is assumed for the methyl terminal group of monomer-5 and monomer-6.

**TABLE 4: Dihedral Angles for Gauche<sup>+</sup> States of Monomeric and Dimeric Model Compounds<sup>a</sup>**

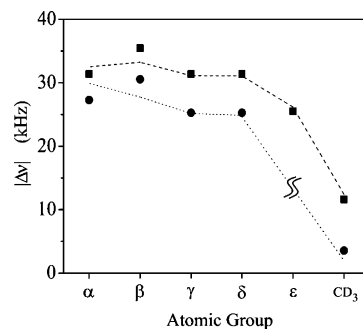
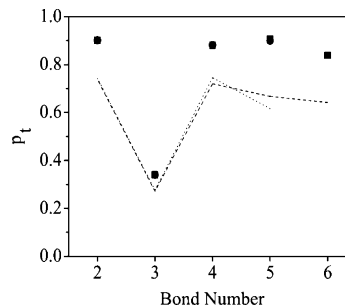
bond <sup>b</sup>	monomer-5	monomer-6	dimer-3	dimer-4	dimer-5	dimer-6
2	98.5	98.5	98.2	99.6	97.4	99.4
3	116.0	116.0	118.3	116.4	116.8	116.4
4	114.1	114.1		111.4	115.0	113.2
5	114.5	113.4				114.8
6		114.5				

<sup>a</sup> In degrees. Determined from ab initio MO calculations at B3LYP/6-31G(d) level. Dihedral angles for the trans states were set equal to 0°, and those for the gauche<sup>-</sup> states were set to the corresponding negative values. <sup>b</sup> For the bond numbers, see Figure 3. For tetramers-5 and -6, the geometries of dimers-5 and -6 were used, respectively.

the  $S(f_k)$  value. In the simulation, the conformer fractions are calculated from the statistical weight parameters and optimized by the MaxEnt method,<sup>61,62</sup> with the weight parameters,  $\sigma_n$ 's and  $\omega_n$ 's, and the interaction parameter,  $C(T,c)$ , adjusted by the Simplex method.<sup>63</sup> The  $E_{\omega_1}$  value is so large even in the free state that  $\omega_1$  was set equal to zero. For further details of the methodology, see refs 15–18.

**3.6.2. Geometrical Parameters.** X-ray diffraction measurements for the four dimers gave their crystal structures. The geometrical parameters were dependent on the molecular packing and somewhat distorted. Therefore, the bond lengths and bond angles, which were evaluated for the monomers and dimers from ab initio MO calculations at the B3LYP/6-31G(d) level, were averaged prior to use in the above-mentioned simulations (see Table 3), because the B3LYP calculations yielded the geometries accordant with the X-ray data. On the other hand, the dihedral angles were determined at the B3LYP/6-31G(d) level for the individual bonds and compounds (see Table 4). For tetramers-5 and -6, dihedral angles of dimers-5 and -6 were substituted, respectively. The benzene ring has been assumed to be a regular hexagon. All of the aromatic carbons and hydrogens and the ethereal O and C<sub>α</sub> atoms are located on the same plane.

**3.6.3. Monomers.** In Figure 14, the  $|\Delta\nu|$  values of monomers-5 and -6, obtained from the RIS + MaxEnt simulations, are compared with the experiments. In general, the calculations reproduced the experiments well. The calculated bond conformations in the alkoxy tails are plotted in Figure 15, where the dotted and dashed lines were obtained from the energy parameters listed in Table 1. The monomers keep their inherent conformational preferences even in the nematic phase.

**Figure 14.** Quadrupolar splittings of monomer-5- $d_{11}$  (● and ⋯) and monomer-6- $d_{13}$  (■ and - - -) dissolved in MBBA at 25 °C and 2.0 mol %: symbol, observation; line, calculation.**Figure 15.** Bond conformations (trans fractions,  $p_t$ 's) of the alkoxy tails of (a) monomer-5 (● and ⋯) and (b) monomer-6 (■ and - - -): symbol, in MBBA at 25 °C and 2.0 mol %; line, in the free (isolated) state.

The ensemble average  $\langle L \rangle$  of quantities  $L_k$ 's can be obtained from

$$\langle L \rangle = \sum_k^K L_k f_k \quad (11)$$

The orientational order parameter of the molecular Z axis,  $\langle S_{ZZ} \rangle$ , of the solutes at 25 °C and 2.0 mol % was evaluated, and results are as follows: monomer-5, 0.282; monomer-6, 0.324. The longer monomer-6 molecule has a larger  $\langle S_{ZZ} \rangle$  value than monomer-5. Figure 16 illustrates the distribution of molecular lengths ( $A_{Z,k}$ 's) along the Z axis of the conformers (see Figure 7). The  $A_{Z,k}$  value was calculated from the van der Waals radii of Bondi.<sup>51</sup> The average dimension  $\langle A_Z \rangle$  was evaluated from eq 11 with the following results: monomer-5, 13.4 (13.0) Å; monomer-6, 14.3 (13.7) Å. Here, the values in the parentheses represent those for the free state.

**3.6.4. Dimers.** Figure 17 shows results of the simulations for dimers-3, -4, -5, and -6 dissolved in MBBA at 25 °C and 2.0 mol %. For the four dimers, the calculations are in agreement with the observations. The dipolar couplings between the ortho deuteron and meta proton of the phenyl group were concomitantly calculated (values in parentheses are the experimental data): dimer-3, 190 (230) Hz; dimer-4, 330 (410) Hz; dimer-5, 250 (310) Hz; dimer-6, 320 (390) Hz. The calculated values seem to be underestimated. The  $D_{HD}$  value is proportional to  $r_{HD}^{-3}$ , and thus is sensitive to the H $\cdots$ D distance. The geometrical parameters adopted here give an  $r_{DH}$  value of 2.483 Å, whereas the X-ray analysis for the dimers yielded a wide range (2.156–2.383 Å) of  $r_{HD}$ . Adoption of the latter average of 2.273 Å improves the  $D_{DH}$  values to 250 Hz (dimer-3), 430 Hz (dimer-4), 320 Hz (dimer-5), and 420 Hz (dimer-6).

Bond conformations of the ethereal spacers, obtained from the simulations, are plotted in Figure 18. In the nematic solution,

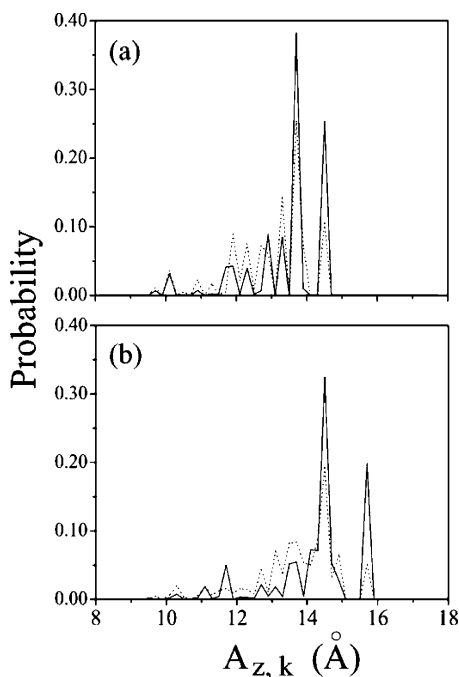


**Figure 16.** Distribution of the conformer length,  $A_{z,k}$ , of (a) monomer-5 and (b) monomer-6: solid line (—), in MBBA at 25 °C and 2.0 mol %; dotted line (⋯), in the free state.

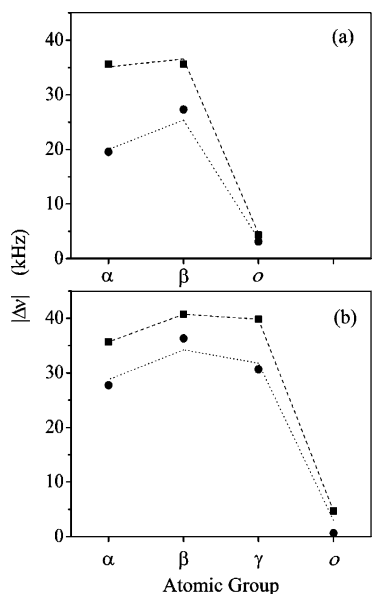


**Figure 17.** Quadrupolar splittings of (a) dimer-3- $d_6$  (● and ⋯) and dimer-4- $d_8$  (■ and ---) and (b) dimer-5- $d_{10}$  (● and ⋯) and dimer-6- $d_{12}$  (■ and ---) dissolved in MBBA at 25 °C and 2.0 mol %: symbol, observation; line, calculation.

the gauche preference of the C–C bond adjacent to the ether linkage is weakened but preserved. Distributions of the molecular dimensions in the Z direction are illustrated in Figure 19. Compared with the dotted lines (free state), the solid lines (nematic state) are generally shifted rightward; the dimers are elongated in the nematic field. Such molecular elongations have been found for polymer LCs.<sup>64–66</sup> For dimer-4 in particular, outstanding changes can be found around 10–11 and 13 Å; the large peaks, mainly due to the conformers with the attractive  $\omega_4$  interactions (Figure 4b), are considerably reduced. This indicates that the crooked  $\omega_4$  conformers rarely occur in the nematic solution. The  $\langle A_z \rangle$  values for the nematic and free states

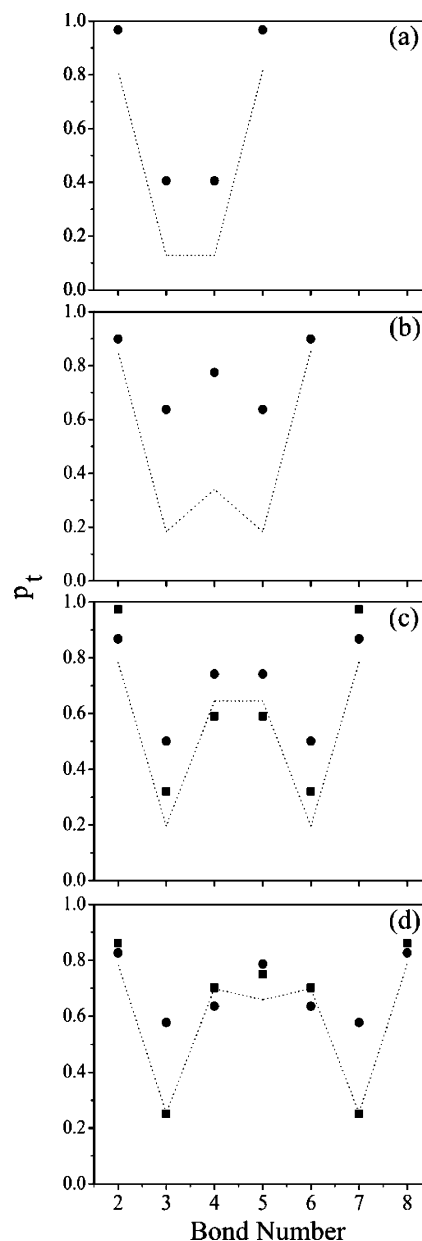


**Figure 18.** Bond conformations (trans fractions,  $p_i$ 's) of the ethereal spacers of (a) dimer-3, (b) dimer-4, (c) dimer-5 (●) and tetramer-5 (■), and (d) dimer-6 (●) and tetramer-6 (■): circle (●) in MBBA at 25 °C and 2.0 mol %; square (■) in PAA at 120 °C and 2.0 mol %; dotted line (⋯), in the free state.

are, respectively, 15.3 and 14.7 Å (dimer-3), 16.8 and 13.6 Å (dimer-4), 16.9 and 15.5 Å (dimer-5), and 17.8 and 17.1 Å (dimer-6).

As a measure of the parallelism of two aromatic rings, the  $\theta$  angle was defined (see Figure 7).<sup>67</sup> The distributions for the four dimers, shown in Figure 20, exhibit a distinct odd–even effect. For dimers-3 and -5, the peaks are concentrated around  $\theta = 30\text{--}90^\circ$ , indicating that the molecules are sharply bent in the nematic solvent. On the contrary, the peaks of dimers-4 and -6 may be divided into two regions:  $0\text{--}30^\circ$  and  $80\text{--}135^\circ$ . For dimer-4, marked differences between the solid and dotted lines are seen in the latter region ( $80\text{--}135^\circ$ ), where the  $\omega_4$  conformers exist. The  $\langle \theta \rangle$  values for the nematic and free states are, respectively, as follows: dimer-3,  $63^\circ$  and  $68^\circ$ ; dimer-4,  $41^\circ$  and  $83^\circ$ ; dimer-5,  $67^\circ$  and  $76^\circ$ ; dimer-6,  $63^\circ$  and  $64^\circ$ . For the reason stated above, dimer-4 shows the largest  $\langle \theta \rangle$  difference between the two states.

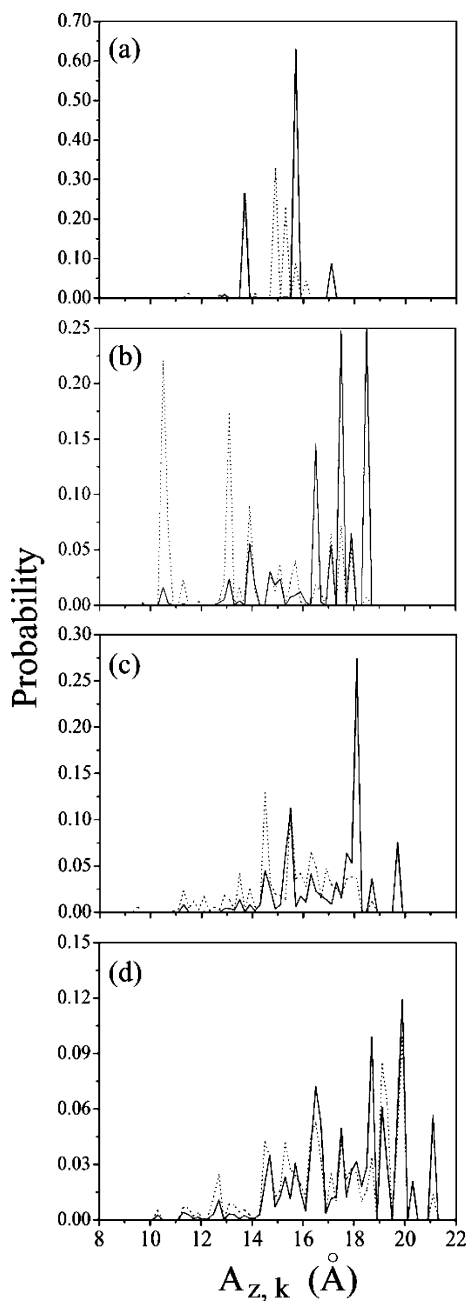


**Figure 19.** Distributions of the conformer length,  $A_{z,k}$ , of (a) dimer-3, (b) dimer-4, (c) dimer-5, and (d) dimer-6: solid line (—), in MBBA at 25 °C and 2.0 mol %; dotted line (···), in the free state.

**3.6.5. Tetramers.** From the similarity in  $^2\text{H}$  NMR between dimer and polymer LCs, the intermolecular orientational correlation has been assumed to persist only up to dimeric units.<sup>67</sup> On this assumption, we have partly adapted the above simulation scheme and applied it to the tetramers. The principal-axis system has been determined only from the central dimeric portion (i.e., the central spacer and two phenylene rings). The principal moments of inertia and the orientational order parameters were evaluated from eqs 5–7, and the simulation was carried out as above.

In Figure 21, the  $|\Delta\nu|$  values thus calculated for tetramers-5 and -6 are compared with the experimental data. In Figure 18, bond conformations of the central spacers are plotted, together with those of dimers-5 and -6. Figure 22 shows the  $\theta$  distributions. For the tetramers, PAA was used as the solvent. However, the results here may be compared with those for the dimers.

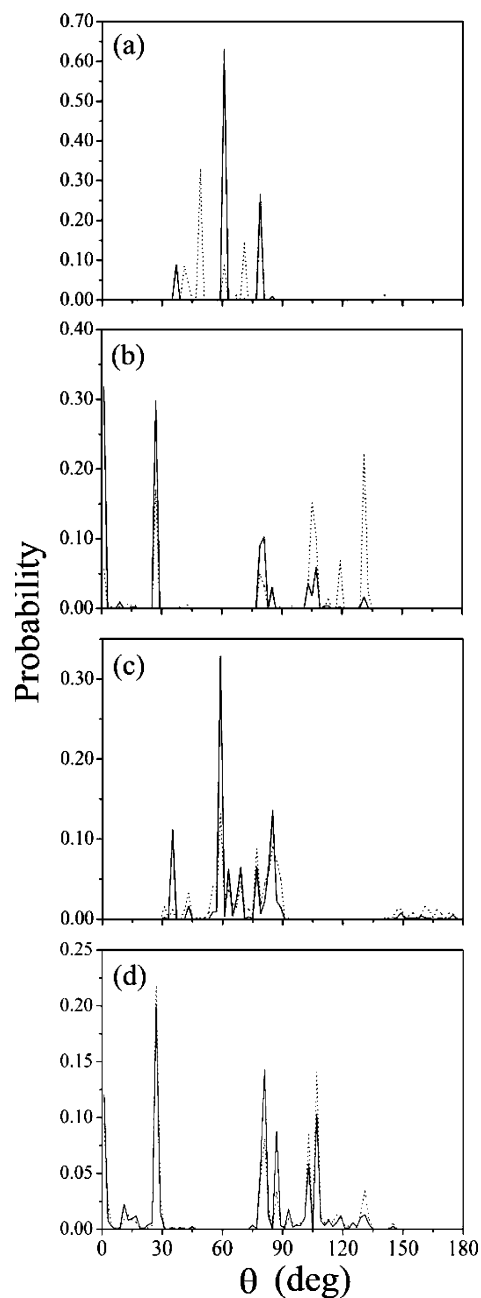


**Figure 20.** Distributions of the  $\theta$  angle of (a) dimer-3, (b) dimer-4, (c) dimer-5, and (d) dimer-6: solid line (—), in MBBA at 25 °C and 2.0 mol %; dotted line (···), in the free state.

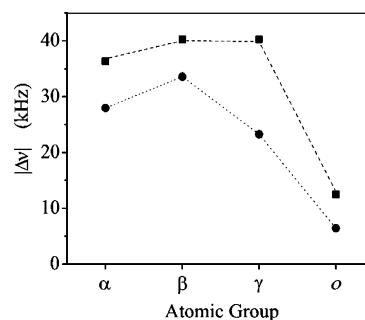


**Figure 21.** Quadrupolar splittings of tetramer-5- $d_{10}$  (● and ···) and tetramer-6- $d_{12}$  (■ and ---) dissolved in PAA at 120 °C and 2.0 mol %: symbol, observation; line, calculation.

The bond conformations appear as if those for the free state (the dotted lines in Figure 18) are somewhat shifted upward.

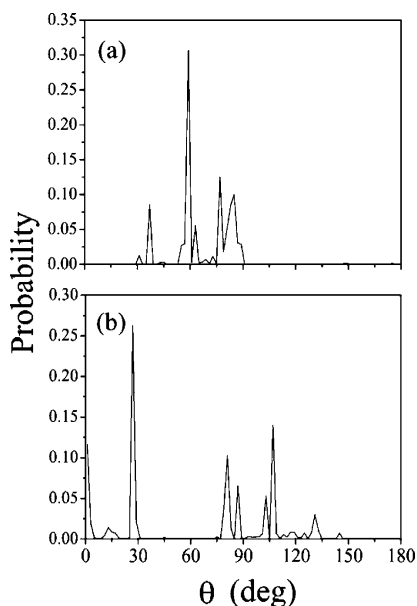


**Figure 22.** Distributions of the  $\theta$  angle of (a) tetramer-5 and (b) tetramer-6 dissolved in PAA at 120 °C and 2.0 mol %.

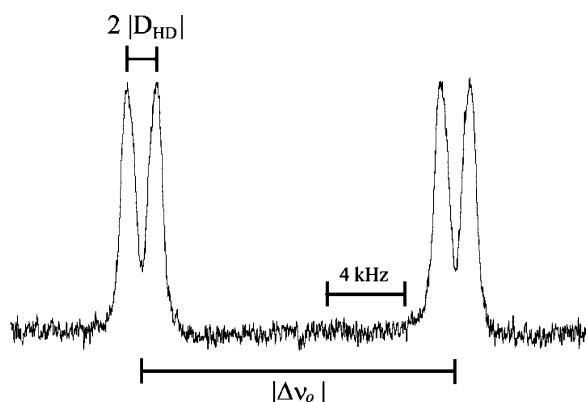


**Figure 23.** Deuterium NMR spectrum observed without  $^1\text{H}$  decoupling from MBBA-2,6- $d_2$  (Figure 1a) mixed in the monomer-5 (2.0 mol %)/MBBA system at 25 °C.

Compared with the dimers, the nematic tetramers seem close to being in the free state. The  $\theta$  distributions of the tetramers are similar to those of the corresponding dimers. However, the small peaks observed around 135–180° for dimer-5 (Figure 20c) completely disappear from the  $\theta$  distribution of tetramer-5. In the nematic field, tetramer-5 may be so long that it does not take the antiparallel arrangement of the phenylene groups, because the arrangement leads to a fold of the molecule. The  $\langle\theta\rangle$  angles for the nematic tetramers-5 and -6 were calculated to be 68° and 61°, respectively.

**3.7. Orientational Orders of Solutes and Solvents.** Figure 23 shows a  $^2\text{H}$  NMR spectrum observed without  $^1\text{H}$  decoupling from MBBA-2,6- $d_2$  (2.0 mol %) mixed in the monomer-5 (2.0 mol %)/MBBA system at 25 °C. A pair of doublets due to the quadrupolar splitting ( $\Delta\nu_o$ ) and dipolar coupling ( $D_{HD}$ ) between the ortho deuteron and meta proton (see Figure 1a) is observed. From the  $D_{HD}$  and  $\Delta\nu_o$  values, orientational order parameters of the phenylene ring were derived as  $S_{ZZ,MBBA}^R = 0.529$  and  $(S_{XX}^R - S_{YY}^R)_{MBBA} = 0.042$ .<sup>68</sup> For the coexistent monomer-5, the above simulation yielded the orientational order parameters of the molecular axes:  $\langle S_{ZZ} \rangle = 0.282$  and  $\langle S_{XX} - S_{YY} \rangle = 0.049$ . The order parameters for the monomer-6/MBBA and dimer/MBBA systems at 25 °C and 2.0 mol % are also listed in Table 5.

**TABLE 5: Orientational Order Parameters of Solutes and Nematic Solvents**

solute	order parameter of solute <sup>a</sup>		order parameter of solvent <sup>b</sup>
	$S_{ZZ}^R$ <sup>c</sup>	$\langle S_{ZZ} \rangle$ <sup>d</sup>	$S_{ZZ}^R$ <sup>c</sup>
monomer-5		0.282	0.529
monomer-6		0.324	0.537
dimer-3	0.193	0.245	0.479
dimer-4	0.339	0.346	0.489
dimer-5	0.255	0.351	0.487
dimer-6	0.318	0.457	0.500
tetramer-5		0.403	0.071
tetramer-6		0.522	0.072

<sup>a</sup> At 2.0 mol %. <sup>b</sup> MBBA at 25 °C for the monomers and dimers; PAA at 120 °C for the tetramers. <sup>c</sup> The order parameter of the para axis of the aromatic ring. <sup>d</sup> The order parameter of the molecular axes.

The  $S_{ZZ}^R$  values of the dimers exhibit a distinct odd–even oscillation. This parameter represents the orientation of the para axis with respect to the nematic director. The  $\langle S_{ZZ} \rangle$  value seems not to be simply proportional to  $S_{ZZ}^R$  of the solute, because the former parameter tends to increase with the chain length. The  $S_{ZZ}^R$  value of MBBA only depends on the solute a little, because both temperature (25 °C) and solute concentration (2.0 mol %) are so low that the orientational order of MBBA is only slightly disturbed. The  $\beta_N^\infty$  values of the dimer/MBBA systems, discussed in section 3.4, are inversely correlated to the  $S_{ZZ}^R$  and  $\langle S_{ZZ} \rangle$  values of the solutes. The tetramers also exhibit an odd–even oscillation in  $\langle S_{ZZ} \rangle$ .

**3.8. Transition Entropies.** For CBA- $x$ 's, the ratios between the NI and CN transition entropies,  $\Delta S_{NI}/\Delta S_{CN}$ , were evaluated from DSC measurements (e.g., 0.05 ( $x = 3$ ), 0.19 ( $x = 4$ ), 0.08 ( $x = 5$ ), and 0.16 ( $x = 6$ )).<sup>25</sup> For polymer LCs,  $[-\text{CO}-\text{C}_6\text{H}_4-\text{O}(\text{CH}_2)_y-\text{O}-\text{C}_6\text{H}_4-\text{COO}-\text{C}_6\text{H}_4-\text{O}(\text{CH}_2)_y-\text{O}-\text{C}_6\text{H}_4-\text{O}-]_n$ , the  $\Delta S_{NI}/\Delta S_{CN}$  ratios for  $x = 3, 4, 5$ , and 6 were, respectively, determined as 0.05, 0.11, 0.08, and 0.17 ( $y = 6$ ) and 0.08, 0.11, 0.09, and 0.14 ( $y = 8$ ).<sup>26</sup> In general, the  $\Delta S_{NI}$  values of LCs are much smaller than  $\Delta S_{CN}$ 's. For CBA-9 and CBA-10, pressure–volume–temperature measurements were carried out, and the isopiestic transitional entropies were divided into the isochoric ( $(\Delta S)_v$ ) and volume-change ( $\Delta S_v$ ) terms.<sup>69,70</sup> The former contribution, mostly due to the conformational change ( $\Delta S^{\text{conf}}$ ) in the spacer, accounts for 40–60%. The above facts indicate that the spacer changes its conformation less in the NI transition than in the CN one. For CBA-9 and CBA-10, the  $(\Delta S_{NI})_v/(\Delta S_{CN})_v$  ratio ( $\sim \Delta S_{NI}^{\text{conf}}/\Delta S_{CN}^{\text{conf}}$ ) was estimated as 15/85.<sup>69,70</sup> If the conformation in the isotropic phase is similar to that in the free state,<sup>71</sup> the above discussion is consistent with the results here.

## 4. Conclusions

The model compounds treated here are not LCs in the narrow sense. Nevertheless, they exhibit distinct odd–even oscillations in  $\beta_N^\infty$ ,  $S_{ZZ}$ 's, and so on, and behave in the nematic solution as if they were LCs. Once a molecule is placed in a nematic field, it reveals its potential liquid crystallinity in the broad sense. The odd–even effect is not peculiar to LCs but common to all chainlike molecules. However, the combination of mesogen and anisotropic field amplifies the effect. In the nematic field, the model compounds keep their inherent conformational preferences, somewhat rigidify and stretch themselves, and turn the aromatic ring toward the nematic director. These compounds act as models for LCs of the corresponding degree of polymerization. The central part of the tetramers may represent the

repeating unit of polymer LCs with the same ethereal spacers. The spacer conformation controls the arrangement of the aromatic rings, the crystal structures, and the thermal properties. The chainlike molecules adjust their spatial configuration to the LC environment, and as a consequence, physical properties of the system are affected. Our simulation scheme for  $^2\text{H}$  NMR has been proven to be applicable to the LC-like molecules with the alternation of a flexible chain and a rigid core.

**Acknowledgment.** We thank Prof. Kishikawa, Dr. Takahashi, Prof. Akutsu, and Dr. Seki of Chiba University for helpful advice on sample preparation and NMR measurements. This work was supported partly by the Izumi Science and Technology Foundation and a Grant-in-Aid for Scientific Research (C) (14550842) from the Japan Society for the Promotion of Science.

**Supporting Information Available:** The  $|\Delta\nu|$  values observed at different temperatures from monomers-5 and -6 and dimers-3, -4, -5, and -6 dissolved in MBBA at 2.0 mol %. This material is available free of charge via the Internet at <http://pubs.acs.org>.

## References and Notes

- Chandrasekhar, S. *Liquid Crystals*, 2nd ed.; Cambridge University Press: New York, 1992.
- de Gennes, P. G.; Prost, J. *The Physics of Liquid Crystals*, 2nd ed.; Oxford University Press: New York, 1993; Chapter 1.
- Kronberg, B.; Gilson, D. F.; Patterson, D. *J. Chem. Soc., Faraday Trans. 2* **1976**, *72*, 1673.
- Kronberg, B.; Patterson, D. *J. Chem. Soc., Faraday Trans. 2* **1976**, *72*, 1686.
- Kronberg, B.; Bassignana, I.; Patterson, D. *J. Phys. Chem.* **1978**, *82*, 1714.
- Martire, D. E. In *The Molecular Physics of Liquid Crystals*; Luckhurst, G. R., Gray, G. W., Eds.; Academic Press: New York, 1979; Chapter 10.
- Oweimreen, G. A.; Martire, D. E. *J. Chem. Phys.* **1980**, *72*, 2500.
- Flory, P. J. *Statistical Mechanics of Chain Molecules*; Interscience: New York, 1969.
- Mattice, W. L.; Suter, U. W. *Conformational Theory of Large Molecules: The Rotational Isomeric State Model in Macromolecular Systems*; Wiley & Sons: New York, 1994.
- Sasanuma, Y.; Abe, A. *Polym. J.* **1991**, *23*, 117.
- Sasanuma, Y. *J. Phys. II* **1993**, *3*, 1759.
- Abe, A.; Iizumi, E.; Sasanuma, Y. *Polym. J.* **1993**, *25*, 1087.
- Sasanuma, Y. *J. Phys. II* **1997**, *7*, 305.
- Skilling, J. In *Maximum Entropy and Bayesian Methods*; Erickson, G. J., Smith, C. R., Eds.; Kluwer: Dordrecht, The Netherlands, 1988.
- Sasanuma, Y. *Polym. J.* **2000**, *32*, 883.
- Sasanuma, Y. *Polym. J.* **2000**, *32*, 890.
- Suzuki, A.; Miura, N.; Sasanuma, Y. *Langmuir* **2000**, *16*, 6317.
- Sasanuma, Y.; Nishimura, F.; Wakabayashi, H.; Suzuki, A. *Langmuir* **2004**, *20*, 665.
- van der Est, A. J.; Kok, M. Y.; Burnell, E. E. *Mol. Phys.* **1987**, *60*, 397.
- Photinos, D. J.; Samulski, E. T.; Toriumi, H. *J. Phys. Chem.* **1990**, *94*, 4688, 4694.
- Rosen, M. E.; Rucker, S. P.; Schmidt, C.; Pines, A. *J. Phys. Chem.* **1993**, *97*, 3858.
- Alejandre, J.; Emsley, J. W.; Tidesley, D. J.; Carlson, P. *J. Chem. Phys.* **1994**, *101*, 7027.
- Luzar, M.; Rosen, M. E.; Caldarelli, S. *J. Phys. Chem.* **1996**, *100*, 5098.
- Sasanuma, Y.; Nakamura, M.; Abe, A. *J. Phys. Chem.* **1993**, *97*, 5155.
- Emsley, J. W.; Luckhurst, G. R.; Shilstone, G. N.; Sage, I. *Mol. Cryst. Liq. Cryst.* **1984**, *102*, 223.
- Griffin, A. C.; Havens, S. J. *J. Polym. Sci., Polym. Phys. Ed.* **1981**, *19*, 951.
- Abe, A. *Macromolecules* **1984**, *17*, 2280.
- Blumstein, A.; Gauthier, M. M.; Thomas, O.; Blumstein, R. B. *Faraday Discuss. Chem. Soc.* **1985**, *79*, 33.
- Sirigu, A. In *Liquid Crystallinity in Polymers: Principles and Fundamental Properties*; Ciferri, A., Ed.; VCH Publishers: New York, 1991; Chapter 7.
- Frisch, M. J.; Trucks, G. W.; Schlegel, H. B.; Scuseria, G. E.; Robb, M. A.; Cheeseman, J. R.; Zakrzewski, V. G.; Montgomery, J. A., Jr.; Stratmann, R. E.; Burant, J. C.; Dapprich, S.; Millam, J. M.; Daniels, A. D.; Kudin, K. N.; Strain, M. C.; Farkas, O.; Tomasi, J.; Barone, V.; Cossi, M.; Cammi, R.; Mennucci, B.; Pomelli, C.; Adamo, C.; Clifford, S.; Ochterski, J.; Petersson, G. A.; Ayala, P. Y.; Cui, Q.; Morokuma, K.; Malick, D. K.; Rabuck, A. D.; Raghavachari, K.; Foresman, J. B.; Cioslowski, J.; Ortiz, J. V.; Stefanov, B. B.; Liu, G.; Liashenko, A.; Piskorz, P.; Komaromi, I.; Gomperts, R.; Martin, R. L.; Fox, D. J.; Keith, T.; Al-Laham, M. A.; Peng, C. Y.; Nanayakkara, A.; Gonzalez, C.; Challacombe, M.; Gill, P. M. W.; Johnson, B. G.; Chen, W.; Wong, M. W.; Andres, J. L.; Head-Gordon, M.; Replogle, E. S.; Pople, J. A. *Gaussian 98*, revision A.11; Gaussian, Inc.: Pittsburgh, PA, 1998.
- Foresman, J. B.; Frisch, M. J. *Exploring Chemistry with Electronic Structure Methods*, 2nd ed.; Gaussian, Inc.: Pittsburgh, PA, 1996.
- Pople, J. A.; Scott, A. P.; Wong, M. W.; Radom, L. *Isr. J. Chem.* **1993**, *33*, 345.
- The deuterations here are partly based on: Zimmermann, H. *Liq. Cryst.* **1989**, *6*, 591.
- Hurd, C. D.; McNamee, R. W. *J. Am. Chem. Soc.* **1932**, *54*, 1648.
- Preparation of 1,5-bis(*p*-hydroxyphenoxy)pentane- $d_{10}$  is partly based on: Tamura, M.; Usui, M.; Hamada, K. (Sumitomo Chemical). Jpn. Kokai Tokkyo Koho 11030, 1991.
- Hsi, S.; Zimmermann, H.; Luz, Z. *J. Chem. Phys.* **1978**, *69*, 4126.
- gNMR*, version 4.1; Cherwell Scientific Ltd.: Oxford, U.K., 1995.
- teXsan: TEXRAY Structure Analysis Package*; Molecular Structure Corporation: The Woodlands, TX, 1985 and 1999.
- Juaristi, E. *Introduction to Stereochemistry and Conformational Analysis*; Wiley & Sons: New York, 1991; Chapter 18.
- Juaristi, E.; Cuevas, G. *The Anomeric Effect*; CRC Press: Boca Raton, FL, 1995; Chapter 4.
- Abe, A.; Jernigan, R. L.; Flory, P. J. *J. Am. Chem. Soc.* **1966**, *88*, 631.
- Tsuzuki, S.; Uchimarui, T.; Tanabe, K.; Hirano, T. *J. Phys. Chem.* **1993**, *97*, 1346.
- Jaffe, R. L.; Smith, G. D.; Yoon, D. Y. *J. Phys. Chem.* **1993**, *97*, 12745.
- Sasanuma, Y.; Ohta, H.; Touma, I.; Matoba, H.; Hayashi, Y.; Kaito, A. *Macromolecules* **2002**, *35*, 3748.
- Sasanuma, Y. In *Annual Reports on NMR Spectroscopy*; Webb, G. A., Ed.; Academic Press: New York, 2003; Vol. 49, Chapter 5.
- Sasanuma, Y. *Macromolecules* **1995**, *28*, 8629.
- Law, R. V.; Sasanuma, Y. *Macromolecules* **1998**, *31*, 2335.
- Sasanuma, Y.; Iwata, T.; Kato, Y.; Kato, H.; Yarita, T.; Kinugasa, S.; Law, R. V. *J. Phys. Chem. A* **2001**, *105*, 3277.
- Law, R. V.; Sasanuma, Y. *J. Chem. Soc., Faraday Trans.* **1996**, *92*, 4885.
- Because the dimeric model compounds treated here have two phenyl rings (i.e.,  $\text{sp}^2$  carbons), the  $V_2^*$  values were not calculated directly from van der Waals radii of Bondi.<sup>51</sup> For three chain molecules (*n*-octane, *n*-dodecane, and *n*-hexadecane), three branched molecules (2,2,4-trimethylpentane, 2,2,4,6,6-pentamethylheptane, and 2,2,4,4,6,8,8-heptamethylnonane), and the four dimers, molecular volumes ( $V_2^{\text{MO}}$ ) larger than 0.001 electrons/bohr<sup>3</sup> were evaluated from ab initio MO calculations at the HF/6-31G(d) level. The conversion ratio from  $V_2^{\text{MO}}$  to the van der Waals volume ( $V_2^*$ ) of Bondi was estimated from the  $V_2^{\text{MO}}$  and  $V_2^*$  values of the three chain molecules and three branched molecules to be 0.733. The  $V_2^*$  values of the four dimers were calculated from  $V_2^* = 0.733V_2^{\text{MO}}$  to be 127.6 cm<sup>3</sup> mol<sup>-1</sup> (dimer-3), 141.5 cm<sup>3</sup> mol<sup>-1</sup> (dimer-4), 155.3 cm<sup>3</sup> mol<sup>-1</sup> (dimer-5), and 169.2 cm<sup>3</sup> mol<sup>-1</sup> (dimer-6).
- Bondi, A. *J. Phys. Chem.* **1964**, *68*, 441.
- The intensity ratios of the outer to inner splittings in Figure 9c were estimated as 1.0, 2.3, 1.0, and 2.0. The second peaks may include signals from three methylene units. Monomer-6- $\alpha$ - $d_2$  was also prepared, but the impurities could not be completely removed. However, a  $^2\text{H}$  NMR spectrum (not shown) of monomer-6- $d_{13}$  + monomer-6- $\alpha$ - $d_2$  indicated that the signal from the  $\alpha$  methylene group is included in the largest peaks.
- Dong, R. Y. *Nuclear Magnetic Resonance of Liquid Crystals*; Springer-Verlag: New York, 1994.
- Greenfield, M. S.; Vold, R. L.; Vold, R. R. *J. Chem. Phys.* **1985**, *83*, 1440.
- Emsley, J. W.; Longeri, M. *Mol. Phys.* **1981**, *42*, 315.
- Anderson, J. M. *J. Magn. Reson.* **1971**, *4*, 231.
- Burnell, E. E.; de Lange, C. A. *Chem. Rev.* **1998**, *98*, 2359.
- Samulski, E. T. *Ferroelectrics* **1980**, *30*, 83.
- Schmidt-Rohr, K.; Spiess, H. W. *Multidimensional Solid-State NMR and Polymers*; Academic Press: New York, 1994; Chapter 2.
- See, for example: Berardi, R.; Spinozzi, F.; Zannoni, C. *J. Chem. Soc., Faraday Trans.* **1992**, *88*, 1863.

- (61) Gull, S. F.; Charter, M.; Skilling, J. *MemSys5*, version 1.20; Maximum Entropy Data Consultants Ltd.: Cambridge, U.K., 1990 and 1991.
- (62) Gull, S. F.; Skilling, J. *Quantified Maximum Entropy MemSys5 User's Manual*; Maximum Entropy Data Consultants Ltd.: Cambridge, U.K., 1991.
- (63) Nelder, J. A.; Mead, R. *Comput. J.* **1965**, *7*, 308.
- (64) Yoon, D. Y.; Bruckner, S. *Macromolecules* **1985**, *18*, 651.
- (65) Bruckner, S.; Scott, J. C.; Yoon, D. Y.; Griffin, A. C. *Macromolecules* **1985**, *18*, 2709.
- (66) Yoon, D. Y.; Bruckner, S.; Volksen, W.; Scott, J. C.; Griffin, A. C. *Faraday Discuss. Chem. Soc.* **1985**, *79*, 41.
- (67) Abe, A.; Furuya, H. *Macromolecules* **1989**, *22*, 2982.
- (68) Emsley, J. W.; Hamilton, K.; Luckhurst, G. R.; Sundholm, F.; Timimi, B. A.; Turner, D. L. *Chem. Phys. Lett.* **1984**, *104*, 136.
- (69) Abe, A.; Nam, S. Y. *Macromolecules* **1995**, *28*, 90.
- (70) Abe, A.; Furuya, H.; Shimizu, R. N.; Nam, S. Y. *Macromolecules* **1995**, *28*, 96.
- (71) Conformational energies of poly(ethylene oxide) and its model compounds largely depend on the medium.<sup>44,45,72</sup> For example, the first-order interaction energy for the C–C bond has been evaluated as follows: gas phase,  $-0.1 \text{ kcal mol}^{-1}$ ;<sup>45</sup>  $\Theta$  state,  $-0.5 \text{ kcal mol}^{-1}$ ;<sup>73</sup> in water,  $-1.2 \text{ kcal mol}^{-1}$ .<sup>74</sup> Therefore, the MO energies shown in Table 1 may not be directly applied to the ethereal spacers in the isotropic phase. However, it is interesting to note that the MO energies of monomers-5 and -6 and dimers-5 and -6 are close to the conformational energies of poly(ethylene oxide) in the  $\Theta$  state:  $E_{\sigma_2} = 0.9$ ,  $E_{\sigma_3} = -0.5$ , and  $E_{\omega_4} = 0.4 \text{ kcal mol}^{-1}$ .<sup>73</sup>
- (72) Abe, A.; Furuya, H.; Mitra, M. K.; Hiejima, T. *Comput. Theor. Polym. Sci.* **1998**, *8*, 253.
- (73) Abe, A.; Mark, J. E. *J. Am. Chem. Soc.* **1976**, *98*, 6468.
- (74) Tasaki, K.; Abe, A. *Polym. J.* **1985**, *17*, 641.